bioRxiv preprint doi: https://doi.org/10.1101/161646; this version posted July 10, 2017. The copyright holder for this preprint (which was not certified by peer review) is the author/funder, who has granted bioRxiv a license to display the preprint in perpetuity. It is made available under aCC-BY-NC-ND 4.0 International license.

Transcriptional responses of *Escherichia coli* during recovery from inorganic or organic mercury exposure

Stephen LaVoie (slavoie5@uga.edu) and Anne O. Summers* (summers@uga.edu)

Department of Microbiology, University of Georgia, Athens, Georgia 30602

Keywords: longitudinal RNA-Seq, transcriptomics, toxic metals, essential metals, stress response, biofilm, phenylmercury, antibiotic resistance

bioRxiv preprint doi: https://doi.org/10.1101/161646; this version posted July 10, 2017. The copyright holder for this preprint (which was not certified by peer review) is the author/funder, who has granted bioRxiv a license to display the preprint in perpetuity. It is made available under aCC-BY-NC-ND 4.0 International license.

ABSTRACT

Background: The protean chemical properties of mercury have long made it attractive for diverse applications, but its toxicity requires great care in its use, disposal, and recycling. Mercury occurs in multiple chemical forms, and the molecular basis for the distinct toxicity of its various forms is only partly understood. Global transcriptomics applied over time can reveal how a cell recognizes a toxicant and what cellular subsystems it marshals to repair and recover from the damage. The longitudinal effects on the transcriptome of exponential phase *E. coli* were compared during sub-acute exposure to mercuric chloride ($HgCl_2$) or to phenylmercuric acetate (PMA) using RNA-Seq.

Results: Differential gene expression revealed common and distinct responses to the mercurials throughout recovery. Cultures exhibited growth stasis immediately after each mercurial exposure but returned to normal growth more quickly after PMA exposure than after $HgCl_2$ exposure. Correspondingly, PMA rapidly elicited up-regulation of a large number of genes which continued for 30 min, whereas fewer genes were up-regulated early after $HgCl_2$ exposure only some of which overlapped with PMA up-regulated genes. By 60 min gene expression in PMA-exposed cells was almost indistinguishable from unexposed cells, but $HgCl_2$ exposed cells still had many differentially expressed genes. Relative expression of energy production and most metabolite uptake pathways declined with both compounds, but nearly all stress response systems were up-regulated by one or the other mercurial during recovery.

Conclusions: Sub-acute exposure influenced expression of ~45% of all genes with many distinct responses for each compound, reflecting differential biochemical damage

bioRxiv preprint doi: https://doi.org/10.1101/161646; this version posted July 10, 2017. The copyright holder for this preprint (which was not certified by peer review) is the author/funder, who has granted bioRxiv a license to display the preprint in perpetuity. It is made available under aCC-BY-NC-ND 4.0 International license.

by each mercurial and the corresponding resources available for repair. This study is the first global, high-resolution view of the transcriptional responses to any common toxicant in a prokaryotic model system from exposure to recovery of active growth. Many genes encoding the responses provoked by these two mercurials are highly conserved evolutionarily, affording insights about how higher organisms may respond to these ubiquitous metal toxicants.

BACKGROUND

The common metallic element mercury (Hg) has no beneficial biological function but its chemical similarities to essential transition metals such as zinc, copper, and iron make it highly toxic to all living systems. Global mercury emissions range from 6500 to 8500 Mg annually with estimates of 50% [1, 2] and even two-thirds [3] being anthropogenic and the rest from volcanism. Mercury exists in multiple chemical forms that are readily susceptible to abiotic and biotic inter-conversions [4]. Mercury occurs naturally as the insoluble HgS ore (cinnabar), as inorganic complexes of Hg^{+2}, Hg^{+1}, or $(Hg_2)^{2+}$ of varying solubility depending on available ligands, and as organomercurials generated by microbial and anthropogenic processes.

Major sources of chronic mercury exposure in humans include dental amalgam fillings [5, 6], consumption of fish containing methylmercury [7], and artisanal gold mining operations [8]. Organomercurials, like phenylmercury, methylmercury, and merthiolate (ethylmercury) have historically been used in medical, industrial and agricultural applications as antimicrobial or fungicidal agents [9-11]. The toxic effects of

bioRxiv preprint doi: https://doi.org/10.1101/161646; this version posted July 10, 2017. The copyright holder for this preprint (which was not certified by peer review) is the author/funder, who has granted bioRxiv a license to display the preprint in perpetuity. It is made available under aCC-BY-NC-ND 4.0 International license.

mercury exposure in humans are associated with neurological, kidney, liver, gastrointestinal, and developmental disorders [9, 12-15].

Like other common electrophilic toxic metals such as arsenic, cadmium, and lead, there is no single biochemical target for mercury damage. Mercury has a strong affinity for sulfur and selenium [16, 17] and therefore targets the cellular thiol pool, composed of glutathione and cysteine thiol groups of proteins [9] and selenocysteine, a rare but critical amino acid in proteins involved in redox defense and thyroid function [18]. Depletion of the cellular thiol pool and disruption of the cellular membrane potential by mercury can induce oxidative stress and apoptosis pathways in mitochondria [19, 20]. However, there is no evidence that mercury itself undergoes Fenton-type chemistry to generate reactive oxygen species like iron and copper [21].

In earlier work we used global proteomics to identify stable mercury-protein binding sites in growing *E. coli* cells exposed to acute levels of organic or inorganic Hg [22]. We found cysteine sites in several hundred proteins, many highly conserved evolutionarily, that formed stable adducts with one or more of these mercurials, consequently disrupting many cellular processes such as iron homeostasis and the electrolyte balance [23]. Importantly, we found that organic and inorganic mercurials had distinct effects on these cellular processes and distinct protein structural preferences. Although the pathobiology of organic and inorganic mercurials has been known for decades to differ, with methyl- and ethyl-mercury recognized as neurotoxic and inorganic mercury as neurotoxic, nephrotoxic, hepatotoxic, and immunotoxic, no previous studies at that time had assessed the biochemical underpinnings of these distinctions on a global scale in any model system.

bioRxiv preprint doi: https://doi.org/10.1101/161646; this version posted July 10, 2017. The copyright holder for this preprint (which was not certified by peer review) is the author/funder, who has granted bioRxiv a license to display the preprint in perpetuity. It is made available under aCC-BY-NC-ND 4.0 International license.

Motivated by our proteomics observations and by microarray data from *C. elegans* showing distinct transcriptional single end point response and toxicity for inorganic and organic mercurials [24], we applied RNA-Seq to examine the transcriptional effects of $HgCl_2$ and phenylmercuric acetate (PMA) exposure on *E. coli* K-12 MG1655 over time. This is the first study to examine the transcriptional response to mercury exposure in a microorganism and the only study to compare directly the effects of different compounds over time through recovery. The changes in gene expression were idiosyncratic for each compound, confirming and extending the idea that the cell suffers overlapping but distinct biochemical damage and marshals both distinct and overlapping recovery processes in response to these chemically distinct mercurials. Although our work was in a bacterium, the high evolutionary conservation of many of the proteins we identified as mercury-vulnerable offers insights for the toxicology of mercury compounds in higher organisms.

METHODS

Cell cultures.

For each biological RNA-Seq replicate *E coli* K-12 MG1655 was subcultured from cryostorage on Luria-Bertani (LB) agar overnight at 37°C. A half-dozen well-isolated colonies were used to inoculate a 20 ml starter culture in Neidhardt MOPS Minimal Medium (NM3) [25] (0.2% final glucose concentration) supplemented with 20 mg/L uracil and 500 µg/L thiamine, which was incubated at 37°C with shaking at 250 rpm overnight (~18 hr). The overnight starter culture was diluted 1:30 to initiate the experimental culture and divided into three 500 ml flasks with 100 ml NM3 in each,

bioRxiv preprint doi: https://doi.org/10.1101/161646; this version posted July 10, 2017. The copyright holder for this preprint (which was not certified by peer review) is the author/funder, who has granted bioRxiv a license to display the preprint in perpetuity. It is made available under aCC-BY-NC-ND 4.0 International license.

which were incubated at 37°C with shaking at 250 rpm. When cultures reached OD_{595} ≈ 0.470 (~ 200 min), two cultures were made 3 μM mercuric chloride ($HgCl_2$) or 3 μM phenylmercuric acetate (PMA) and the third was left as an unexposed control. Mercury stocks were prepared fresh for each growth experiment: 10 mM $HgCl_2$ (Fisher) in water and 5 mM PMA (Sigma) in 25% dimethyl sulfoxide DMSO (Fisher), which is 2.1 mM or 0.015% v/v final concentration DMSO in culture. These mercurial exposures were chosen from prior pilot experiments to find exposure conditions (OD_{595}, mercurial concentration and sampling times) that displayed a marked decrease in growth rate relative to the unexposed control but allowed subsequent restoration of rapid growth rate (i.e. recovery) within 1 hr (approximately one generation in NM3) after mercurial exposure. Duplicate 1-ml aliquots of each culture were collected at 0 (unexposed control only), 10, 30, 60 min after mercurial exposure and immediately centrifuged at 20,800 *x g* for 3 min at 4°C. Spent medium was aspirated and cell pellets were frozen at -70°C within 5 min after collection. Seven biological replicates were prepared following this protocol and the average variance for all replicates in culture optical density over each 90-min experiment ranged from 0.0019 – 0.0073. The three biological replicates with the lowest variance between growth curves (range from 0.0007 – 0.0017 for all time points) were prepared for RNA-Seq.

Purification of mRNA

One cell pellet from each condition and sampling time was thawed on ice; total RNA was isolated by RNA*snap*™ [26] and stored at -70°C. DNA contamination was removed by two treatments with Turbo-DNase (Ambion; Life Technologies). RNA

bioRxiv preprint doi: https://doi.org/10.1101/161646; this version posted July 10, 2017. The copyright holder for this preprint (which was not certified by peer review) is the author/funder, who has granted bioRxiv a license to display the preprint in perpetuity. It is made available under aCC-BY-NC-ND 4.0 International license.

concentrations and A_{260}/A_{280} ratios were determined using a Nanodrop™ 1000 spectrophotometer (Thermo Scientific). Ribosomal RNA depletion was performed with the Ribo-Zero™ rRNA removal kit for Gram-negative bacteria (Epicentre) and concentrated using RNA Clean and Concentrator™ -5 columns (Zymo Research) following the manufacturer's instructions. Purified mRNA was quantified using the Nanodrop™ and stored at -70°C.

Library Preparation and Next-generation Sequencing

The quality and quantity of rRNA-depleted RNA was assessed on a 2100 Bioanalyzer RNA pico chip (Agilent Technologies) using the manufacturer's recommendations. Next-generation sequencing (NGS) libraries were prepared using the Kapa biosystems NGS stranded library prep kit for RNA-Seq with dual indexed Illumina adapters. Library insert size was ~150 bp, as determined by high-sensitivity NGS fragment analysis kit for Fragment Analyzer™ (Advanced Analytical Technologies) using the manufacturer's instructions. Quantification of each library was done by qPCR and all 30 libraries were pooled in equal concentrations. The library preparation, quality analysis, and pooling were performed by the Georgia Genomics Facility (http://dna.uga.edu). Paired-end (2 x 50 bp) sequencing of the pooled libraries using the Illumina HiSeq 2000 platform was performed by the HudsonAlpha Institute for Biotechnology Genomic Services Laboratory (http://gsl.hudsonalpha.org). See Table S1 for index and filename information for data uploaded to NCBI Gene Expression Omnibus database (http://www.ncbi.nlm.nih.gov/geo/) with accession ID: GSE95575.

bioRxiv preprint doi: https://doi.org/10.1101/161646; this version posted July 10, 2017. The copyright holder for this preprint (which was not certified by peer review) is the author/funder, who has granted bioRxiv a license to display the preprint in perpetuity. It is made available under aCC-BY-NC-ND 4.0 International license.

Data Processing and Differential Expression Analysis

Quality control processing of sequence data was performed using Galaxy (https://galaxyproject.org) on the Georgia Advanced Computing Resource Center at the University of Georgia. The FASTX tools in Galaxy (http://hannonlab.cshl.edu/fastx_toolkit) were used for filtering by quality (80% of sequence ≥ quality score of 20), then reads were trimmed at both 5' and 3' ends using a window and step size of 1 with quality score ≥ 20. Forward- and reverse-read mate-pairs were assembled and aligned to the *Escherichia coli* MG1655 K-12 genome using Bowtie2 [27]. SAMtools [28] was used to convert Bowtie2 output (.bam file) to SAM format. The number of sequence reads that aligned to features in the annotation file (Escherichia_coli_str_k_12_substr_mg1655.GCA_000005845.2.24.gtf from http://bacteria.ensembl.org) were tabulated from the resulting SAM alignment files using the HTSeq-count program [29] with intersection non-empty mode. Mapped read counts were analyzed for differential expression (false discovery rate of ≤ 0.01, fold-change ≥ 2) using the baySeq package in R [30]. Within baySeq, two-way comparisons using quantile normalization were made for all three biological replicate transcriptomes over time for $HgCl_2$ exposure or PMA exposure versus the unexposed control. We also examined changes over time in the unexposed control culture itself.

RESULTS

Effects of sub-acute mercury exposure on growth of MG1655.

We defined sub-acute exposure as the concentration of mercury that clearly inhibited growth relative to the unexposed control but allowed cells to resume growth

bioRxiv preprint doi: https://doi.org/10.1101/161646; this version posted July 10, 2017. The copyright holder for this preprint (which was not certified by peer review) is the author/funder, who has granted bioRxiv a license to display the preprint in perpetuity. It is made available under aCC-BY-NC-ND 4.0 International license.

184 within 1 hour or approximately one generation in this medium (Figure 1a, Figure S1).
185 Based on pilot experiments the appropriate dose proved to be 3 μM for both mercurials.
186 Exposure to 4 - 5 μM $HgCl_2$ prevented growth resumption during 1 hr and the effects of
187 PMA exposure were similar at 3 and 5 μM; exposure to 2.5 μM of either mercurial did
188 not consistently retard growth (data not shown).
189 Cell-associated Hg (Table S2 and Supp Info Methods) declined slowly as has
190 been reported previously for low level $HgCl_2$ exposure of Hg sensitive cells and was
191 attributed to non-specific endogenous reductants [31-33]. Bound Hg in cells exposed
192 either to $HgCl_2$ or to PMA declined similarly from ~50% of total Hg added to culture at
193 10 min to ~20% at 30 min, after which Hg loss from PMA-exposed cells continued to
194 decline to 11% of input at 60 min. In contrast, cell-associated Hg in cells exposed to
195 $HgCl_2$ increased from 24% at 30 to 47% at 60 min. Presently, we have no simple
196 explanation for this unexpected difference in cell-bound Hg in late exponential phase
197 cultures, however it does echo our finding that cultures acutely exposed to 40μM or 80
198 μM PMA or $HgCl_2$ bound 24% or 208% more Hg(II) than PhHg, respectively [23]. Also
199 notable was a brief drop in the culture optical density immediately after PMA exposure
200 consistent with some cell lysis as has been reported [34]. The lack of apparent lysis
201 after divalent $HgCl_2$ exposure may be due to its ability to cross-link cell envelope
202 proteins via their cysteines, which is not possible for monovalent PMA.
203
204 ***Transcriptome benchmarks***
205 Paired-end libraries averaged over 9.5 million reads and mapped reads provided
206 an average of 143X coverage (Figure S2). The sequencing data were of high quality,

bioRxiv preprint doi: https://doi.org/10.1101/161646; this version posted July 10, 2017. The copyright holder for this preprint (which was not certified by peer review) is the author/funder, who has granted bioRxiv a license to display the preprint in perpetuity. It is made available under aCC-BY-NC-ND 4.0 International license.

requiring removal of only 11% as low-quality reads. Of the high-quality reads, 97% of reads mate-paired, 99.4% of paired reads mapped to the genome and 82% of reads mapped to an annotated genome feature on average from all libraries.

Overall 89% of annotated mapped reads were to coding regions (CDS) based on raw un-normalized read counts per gene output from HTseq-count program [29](Figure S3, Table S3, Table S4). Pearson correlations of raw read counts confirmed that no strong biases were introduced in biological replicates for each condition (Figures S4-S6). That dispersion is slightly greater in both mercury exposure conditions than in unexposed cultures, especially at later time points, is consistent with perturbations of multiple cellular processes.

Mapped reads to rRNA constituted only 0.3% of total reads (std. dev. = 0.425) on average for all libraries (Table S3) consistent with effective Ribo-Zero™ rRNA removal. In the unexposed culture non-coding RNA's (ncRNA) were 4% of total reads over all time points, but their percentage increased in mercury exposure conditions indicating greater differential expression of some ncRNA genes (details below). The very abundant tmRNA (*ssrA*) needed for rescuing stalled ribosomes [35] was 6% of total reads in the unexposed condition and although this percentage increased for mercury exposure conditions, the tmRNA gene (*ssrA*) was not differentially expressed under any condition. Pseudogenes accounted for less than 1% of total reads, but up to 35% ($HgCl_2$) and 13% (PMA) of them were significantly up-regulated. The tRNA's were less than 1% of total reads because the library preparation method we used was not optimized for such small RNAs. However, approximately 35% of these observed tRNA

bioRxiv preprint doi: https://doi.org/10.1101/161646; this version posted July 10, 2017. The copyright holder for this preprint (which was not certified by peer review) is the author/funder, who has granted bioRxiv a license to display the preprint in perpetuity. It is made available under aCC-BY-NC-ND 4.0 International license.

229 genes were significantly down-regulated during the first 30 min after exposure to either
230 mercurial.
231
232 ***$HgCl_2$ and PMA transcriptional responses are not the same.***
233 We expected that differentially expressed genes (DEGs) in the mercury exposure
234 conditions (compared to the unexposed cells) would change over time as the cells
235 transitioned from initial growth stasis back into a normal growth rate. We also expected
236 that some DEG responses would be similar because both mercurials are thiophilic and
237 will bind to the cellular thiol redox buffer, glutathione (GSH), and to protein cysteine
238 residues. However, since there are physiological differences and protein site
239 preferences for each compound in acute Hg(II)- or PMA-exposure [23 and Zink et. al. in
240 preparation] we aimed here at a low exposure using a longitudinal protocol to discern
241 more subtle distinctions between these mercurials as the cells experienced stasis and
242 then recovered their growth rate. In the following sections, we first describe the bulk
243 measures of gene expression over time and then describe differences in specific
244 functional pathways.
245
246 ***Differentially expressed genes: the view from 30,000 feet.***
247 *a. Differentially expressed genes (DEG) for each condition and time point*
248 DEGs were determined by pairwise comparisons of mercury exposure conditions
249 relative to the unexposed culture at the corresponding time point (Figure 1b and Table
250 S5). Ten minutes after exposure, expression of 41% or 49% of the 4,472 non-rRNA
251 genes changed significantly for $HgCl_2$ or PMA-exposed cells, respectively (Figure 1b).

bioRxiv preprint doi: https://doi.org/10.1101/161646; this version posted July 10, 2017. The copyright holder for this preprint (which was not certified by peer review) is the author/funder, who has granted bioRxiv a license to display the preprint in perpetuity. It is made available under aCC-BY-NC-ND 4.0 International license.

252 At 30 min with growth still arrested, 32% of genes in the $HgCl_2$-exposed cells were
253 differentially expressed (Figure 1b), (Figure 1a, red). In contrast, PMA-exposed cells at
254 30 min began to recover their prior growth rate (Figure 1a, green), but 45% of their
255 genes remained differentially expressed (Figure 1b). By 60 min, the PMA-exposed cells
256 were growing at nearly their pre-exposure rate and only 1.5% of genes were
257 differentially expressed, whereas the $HgCl_2$-exposed cells were still growing more
258 slowly than pre-exposure with 13% of their genes still differentially expressed compared
259 to the unexposed cells (Figure 1b).
260
261 *b. Shared and unique genes at each time point for each exposure.*
262 The total distinct DEGs across all time points was slightly lower for $HgCl_2$ (2,327)
263 than for PMA (2,541) exposure (Figure 1b and Figure S7). More striking were the
264 differences in DEGs at each time point; PMA-exposed cells modulated 20% more genes
265 at 10 min (2,181 vs 1,821) and 40% more at 30 min (2,007 vs 1,422) than $HgCl_2$
266 exposed cells. This trend completely reversed by 60 min when DEGs declined in both
267 exposure conditions but $HgCl_2$ exposed cells were still modulating ~9-fold more genes
268 (563) than PMA-exposed cells (65), consistent with the latter recovering normal growth
269 sooner (Figure 1a). Also notable is the carryover of DEGs from one time point to the
270 next where $HgCl_2$ exposed cells have 1,001 DEGs in common at 10 and 30 min after
271 exposure but that number is 65% greater in PMA-exposed cells (1,650) (Figure S7).
272 However, $HgCl_2$ exposed cells have 52% more DEGs that are unique at 10 min
273 compared to PMA-exposed cells (804 vs 529), i.e. more $HgCl_2$ provoked DEGs occur
274 sooner after exposure than later. $HgCl_2$ exposure also yields more DEGs that occur at

bioRxiv preprint doi: https://doi.org/10.1101/161646; this version posted July 10, 2017. The copyright holder for this preprint (which was not certified by peer review) is the author/funder, who has granted bioRxiv a license to display the preprint in perpetuity. It is made available under aCC-BY-NC-ND 4.0 International license.

all time points compared to PMA (Figure S7) since there are very few DEGs at 60 min for PMA exposure.

c. *Up-regulated vs. down-regulated genes for each exposure*

Sorting expression simply into genes up-regulated or down-regulated by $HgCl_2$ or PMA at each time point (Figure 2) revealed additional quantitative distinctions between them. For up-regulated genes, PMA-provoked more unique DEGs than DEGs in common with $HgCl_2$ exposure at all time points, in contrast to $HgCl_2$ which had more DEGs in common than unique at all but the last time point. This trend was not continued for down-regulated genes where more genes were in common for both compounds than unique at all time points.

Thus, early in exposure the cell reduced expression of a similar number of genes for both mercurials, but up-regulated expression of many more genes in response to PMA than to $HgCl_2$, and these distinct trends persisted to the middle time point. By 60 min, gene expression of PMA-exposed cells closely resembled that of unexposed cells, but $HgCl_2$ exposed cells still have many up- and down-DEGs, consistent with slower growth rate recovery by $HgCl_2$ exposed compared to PMA-exposed cells (Figure 1a).

d. Differentially expressed genes grouped by functional category.

To sort our observations from a different perspective, the DEGs for each condition were grouped by Clusters of Orthologous Groups (COGs) to identify expression differences based on gene functions (Figure 3 and Table S6). For most COGs, both mercurials elicited the strongest response, up or down, within the first 10

bioRxiv preprint doi: https://doi.org/10.1101/161646; this version posted July 10, 2017. The copyright holder for this preprint (which was not certified by peer review) is the author/funder, who has granted bioRxiv a license to display the preprint in perpetuity. It is made available under aCC-BY-NC-ND 4.0 International license.

298 min of exposure (Figure 3); in most cases, the responses were of similar magnitude. At
299 30 min, the PMA (green) responses remained nearly the same, up or down, but $HgCl_2$
300 provoked responses (red) generally diminished, often sharply. By 60 min, expression in
301 PMA-exposed cells was barely distinguishable from the unexposed cells in all COG
302 categories, whereas $HgCl_2$ exposed cells had notable differential expression in most
303 COG categories.

304 The four well-defined COG categories with the most DEGs were energy
305 production (C), amino acid metabolism (E), carbohydrate metabolism (G), and
306 transcription (K), which are also categories with a large number of genes (284, 355,
307 381, and 294 respectively) in *E. coli* (Figure 3 legend). COG categories R and S
308 encoding poorly defined (261) or non-defined (203) genes were also represented
309 proportionally. These data suggest both mercurials broadly affect most metabolic
310 categories, albeit to different degrees and at different rates. However, four well-defined
311 COG categories have strikingly different responses to $HgCl_2$ and PMA. COG categories
312 for nucleotide metabolism (F), translation (J), motility (N), and intracellular trafficking (U)
313 have much less up-regulation in $HgCl_2$ exposed cells than in PMA-exposed cells. There
314 are relatively few DEGs involved in cell division (D), extracellular structures (W), and
315 mobile genetic elements (X) and genes within these categories responded similarly to
316 both mercurials. Thus, grouping DEGs by COGs emphasizes the broad functional
317 differences and similarities between $HgCl_2$ and PMA exposure. Furthermore, this
318 approach highlights that DEGs occur in all functional categories for both compounds,
319 but still display distinct differences in transcriptional response to each compound. We
320 provide gene-level detail on several of these functional groups below. Note that the

bioRxiv preprint doi: https://doi.org/10.1101/161646; this version posted July 10, 2017. The copyright holder for this preprint (which was not certified by peer review) is the author/funder, who has granted bioRxiv a license to display the preprint in perpetuity. It is made available under aCC-BY-NC-ND 4.0 International license.

321 COG database only includes functional annotations for 3,398 of *E. coli's* 4,497 genes,
322 but functional categories discussed below in more detail are not limited to COG-
323 annotated genes.

324 A heat map of the DEGs log-fold changes (Figure 4) provides a more granular
325 look at all DEGs for both compounds across all time points. The heat map, using Ward's
326 minimum variance clustering method [36], shows considerable uniformity of up- and
327 down-regulated expression during the 30 min after PMA exposure. In contrast, although
328 $HgCl_2$ exposed cells grossly shared many DEGs with PMA-exposed cells (Figure 2), the
329 heat map reveals a more variegated response to Hg(II) in which different genes are up-
330 or down-regulated at all time points, in contrast to the relatively consistent response of
331 PMA during recovery. Overall, 34% of DEGs are unique to only one mercurial and ~3%
332 of all DEGs had an opposite response to each compound (Table S5). The most
333 dramatic differences were at 60 min when $HgCl_2$ exposed cells were still modulating
334 many genes but PMA-exposed cells had only minor differences with unexposed cells,
335 consistent with their faster recovery of normal growth (Figure 1a). We dissect some of
336 these differences in function-specific heat maps below.

337 We also used STRING (version 10.0) [37, 38] for unsupervised network analysis
338 to identify gene clusters that were up-regulated in response to each compound (Figure
339 S8 and Table S7). We focused on up-regulated genes on the working assumption that
340 they are more likely to contribute to recovery than genes whose expression is turned
341 down. Gene clusters were generated by STRING based on organism specific data
342 mining to identify genes with a functional association, such as a common biological
343 purpose, location within the same operon, or shared regulatory mechanism. Note that

bioRxiv preprint doi: https://doi.org/10.1101/161646; this version posted July 10, 2017. The copyright holder for this preprint (which was not certified by peer review) is the author/funder, who has granted bioRxiv a license to display the preprint in perpetuity. It is made available under aCC-BY-NC-ND 4.0 International license.

this network algorithm does not consider fold-change intensity of response; it enumerates only whether an up-regulated gene is present at a given time point. The up-regulated DEGs (nodes) of $HgCl_2$ exposed cells formed several tight clusters encompassing 16 gene-ontology functions (GOFs) at 10 min, nine GOFs at 30 min, and seven GOFs at 60 min (Figure S8 and Table S7). In contrast, although there were more nodes for PMA-exposure at 10 and 30 min, there were fewer edges yielding no well-defined clusters at 10 min and only two GOFs at 30 min. This network analysis suggests that, although PMA provokes more DEGs than Hg(II) does, there is less functional congruence between the genes involved in the response to PMA. Specific gene and function changes are discussed further in the next section.

Lastly, as a control for using RNA-Seq in a longitudinal experiment, we observed DEGs at sequential time points in the unexposed control culture (Figure S9 and Table S8). As expected, changes were gradual over time with no more than 5% of the genome being differentially expressed from one time point to the next. At the 60 min time point, as the cells approached stationary phase 815 genes were differentially expressed compared to mid-log (time 0). Sorting these DEGs by COGs (Figure S9) and by STRING network analysis (Figure S10 and Table S7) showed, as expected, many DEGs were consistent with normal transitioning from mid-log to early stationary phase [39, 40].

Higher resolution view of expression differences in specific functional groups during recovery from exposure to $HgCl_2$ or PMA

bioRxiv preprint doi: https://doi.org/10.1101/161646; this version posted July 10, 2017. The copyright holder for this preprint (which was not certified by peer review) is the author/funder, who has granted bioRxiv a license to display the preprint in perpetuity. It is made available under aCC-BY-NC-ND 4.0 International license.

366 Taking the perspective that a toxicant is a kind of signaling molecule, we
367 considered differences in gene expression for the two Hg compounds to reflect how the
368 cell senses the biochemically distinct damage produced by these two metallo-
369 electrophiles as manifest by what tools the cell calls upon to restore its viability. A quick
370 snapshot of the great extent of these compound-specific differences can be seen in the
371 genes with a >20-fold increase in differential expression after $HgCl_2$ exposure (Table 1)
372 or PMA exposure (Table 2). Here we emphasize up-regulated genes on the working
373 assumption they could contribute directly or indirectly to repairing damage caused by
374 mercurial exposure. The 25 genes highly up-regulated by $HgCl_2$ (Table 1) are involved
375 in altering the cell surface, oxidative stress response and repair, protein chaperones,
376 metals homeostasis, and ribonucleotide reductase. The vestigial prophage genes likely
377 play no rescue role for the cell and were simply activated by generalized stress
378 responses. The corresponding PMA response echoed only 8 of these 25 $HgCl_2$ high-
379 responders, and notably did not include the vestigial phage genes.
380 For PMA, the highly up-regulated genes are a distinct contrast to those for $HgCl_2$.
381 First, the maximum amplitude of the PMA-provoked differential expression is generally
382 much less than for Hg(II)-provoked high differential expression (Table 1), which could
383 reflect the lower uptake of PMA. Secondly, while 11 of the 17 PMA-provoked genes
384 were also on the $HgCl_2$ highly differential expression list, ion transport and antibiotic
385 resistance loci were more prominent with PMA and prophage genes were absent.
386 These two snapshot tables make the points that both mercurials generate broad,
387 but idiosyncratic, cellular responses. To place these “tips of many icebergs” in their
388 larger cellular context, we used heat maps and tables of subsets of functionally related

bioRxiv preprint doi: https://doi.org/10.1101/161646; this version posted July 10, 2017. The copyright holder for this preprint (which was not certified by peer review) is the author/funder, who has granted bioRxiv a license to display the preprint in perpetuity. It is made available under aCC-BY-NC-ND 4.0 International license.

389 genes to discuss the differential effects of $HgCl_2$ and PMA on twelve canonical cellular
390 systems in the following sections.
391
392 i. INFORMATIONAL MACROMOLECULES
393 *(a) DNA replication, recombination and repair*
394 Of the 24 genes for initiation and maintenance, and termination of chromosome
395 replication, there were more genes down-regulated (8) than up-regulated (3) in
396 response to $HgCl_2$ and an equal number up- or down-regulated genes (7) in response to
397 PMA (Table S9). Of the 14 genes encoding the replicative polymerase holoenzyme, four
398 genes capable of translesion synthesis (*polB*, *dinB*, *umuCD*) were up-regulated more by
399 $HgCl_2$ exposure (Table S9), suggesting a greater degree of direct or indirect DNA
400 damage by $HgCl_2$ exposure. Of the 45 genes for repair and recombination proteins the
401 transcriptional response to each mercurial was very similar (11 up-regulated and 16
402 down-regulated for $HgCl_2$; 9 up-regulated and 18 down-regulated for PMA). But there
403 were repair genes unique to each compound: *xthA*, *uvrAB*, *mutM,* and *recN* were only
404 up-regulated by $HgCl_2$; and *mutH* and *mutY* were only up-regulated by PMA.
405 The *recA, recN,* and *xthA* DNA repair genes were the most highly up-regulated
406 (≥10 fold) in response only to $HgCl_2$. The *recA* gene, induced by double-strand DNA
407 breaks, serves multiple roles in DNA repair [41, 42]. Curiously, expression of *recBCD,*
408 which is needed for break repair, either did not change or declined compared to
409 unexposed cells for both mercurials. Expression of several genes involved in repair
410 (*recG*, *nth*, *hsdS*, and *mcrC*) were down-regulated by both compounds, but with much
411 larger negative fold-changes for PMA than $HgCl_2$. Thus, the cells responded quickly to

bioRxiv preprint doi: https://doi.org/10.1101/161646; this version posted July 10, 2017. The copyright holder for this preprint (which was not certified by peer review) is the author/funder, who has granted bioRxiv a license to display the preprint in perpetuity. It is made available under aCC-BY-NC-ND 4.0 International license.

412 both mercurials, but some distinct responses suggest these two compounds directly or
413 indirectly yield different kinds of DNA damage.
414
415 *(b) Transcription*
416 Of the core RNA polymerase (RNAP) genes only PMA-exposure increased
417 expression of a single gene *rpoZ* (ω subunit), but expression decreased in the
418 remaining *rpoABC* core genes (Table S10). $HgCl_2$ exposure did not change expression
419 of any RNAP core genes except for a transient 3-fold drop in *rpoA* at 30 min. Only one
420 of the five termination factors, the Rho-directed anti-terminator, *rof,* increased and did
421 so for both mercurials with PMA again provoking a greater response.
422 Genes for three sigma factors displayed increased expression upon exposure to
423 either mercurial, with *rpoH* (heat shock sigma factor) and *rpoS* (stationary phase and
424 stress response sigma factor) increasing more following PMA-exposure and *rpoD*
425 (housekeeping sigma factor) only increasing after $HgCl_2$ exposure. The effects of $HgCl_2$
426 or PMA exposure on the regulation of genes within each regulon controlled by *E. coli's*
427 seven sigma factors are tabulated in Table S11. Many genes are modulated
428 differentially by $HgCl_2$ or PMA-exposure, but no single sigma factor is uniquely
429 responsible for increases or decreases in responses to these two compounds.
430 Many of the 203 transcriptional regulators annotated in the RegulonDB (Table 3)
431 [43, 44] and the 1,723 genes they control were expressed differently with the two
432 mercurials (Table S12). PMA provoked up-regulation of significantly more transcription
433 factor genes at 10 and 30 min than $HgCl_2$ exposure, but slightly fewer down-regulated
434 regulators (Table 3). Of all COG categories, transcription had the most up-regulated

bioRxiv preprint doi: https://doi.org/10.1101/161646; this version posted July 10, 2017. The copyright holder for this preprint (which was not certified by peer review) is the author/funder, who has granted bioRxiv a license to display the preprint in perpetuity. It is made available under aCC-BY-NC-ND 4.0 International license.

435 genes for both mercurials (Figure 3 and Table S6). PMA up-regulated ~40% more
436 transcription related genes at 10 min and ~80% more genes at 30 min than $HgCl_2$. Six
437 activators (*mhpR, glcC, gadX, soxS, mlrA, phoB*) and three repressors (*mcbR, iscR,*
438 *betI*) were up at all times for $HgCl_2$, but *gadX* was the only activator gene up-regulated
439 at all times for both mercurials (Table S12). GadX is part of the RpoS regulon [45] and
440 activates the acid resistance system and multidrug efflux [46, 47]. Details of
441 transcription factors and their regulons are provided in Table S12.

442 Lastly, *E. coli* has 65 currently annotated (ASM584v2), small non-coding RNAs.
443 Although our RNA purification and library preparation methods were not optimized for
444 their enrichment, we observed differential expression for a number of them (Table S5,
445 feature type "ncRNA"). ncRNAs up-regulated for both mercurials are involved in
446 regulation of acid resistance (*gadY*), oxidative stress (*oxyS*), and multiple transporters
447 (*gcvB* and *sgrS*). In contrast, adhesion and motility (*cyaR*), and anaerobic metabolism
448 shift (*fnrS*) were down-regulated by both compounds.
449
450 *(c) Translation*

451 Upon $HgCl_2$ exposure 83% and 74% of ribosomal proteins (r-proteins) were
452 down-regulated at 10 and 30 min, respectively, versus only 4% and 41% for PMA at the
453 corresponding times (Figures 5 and S9; data for all functional group heat maps are
454 shown in Table S13 and Table S14). Transcription of r-proteins is repressed directly by
455 binding of the nutritional stress-induced nucleotide ppGpp and DksA protein to RNAP
456 [48]. The ppGpp synthase genes, *spoT* and *relA*, were down-regulated or unchanged,
457 but expression of *dksA* was up-regulated for both $HgCl_2$ and PMA exposure. R-protein

bioRxiv preprint doi: https://doi.org/10.1101/161646; this version posted July 10, 2017. The copyright holder for this preprint (which was not certified by peer review) is the author/funder, who has granted bioRxiv a license to display the preprint in perpetuity. It is made available under aCC-BY-NC-ND 4.0 International license.

458 expression can also be inhibited by excess r-proteins binding to and inhibiting
459 translation of their own mRNAs [49, 50].

460 Translation initiation and elongation factors were largely unchanged, but
461 expression of all three peptide chain release factor genes were down for PMA and the
462 ribosome recycling factor (*frr*) was up only for PMA, consistent with interruption of
463 translation. Eight tRNA-synthase genes declined with $HgCl_2$ but PMA caused only four
464 tRNA-synthase genes to decline and two to increase in expression (Table S14). Both
465 mercurials caused a relative decline in tRNA expression for most amino acids,
466 especially arginine, lysine, methionine, tyrosine, and valine tRNAs. With very few
467 exceptions ribosome assembly and translation were shut down for up to 30 min by both
468 compounds but returned to normal levels by 60 min.

469

470 *(d) Macromolecular turnover and chaperones*

471 Divalent inorganic mercury can stably crosslink proteins and their subdomains
472 via cysteines, disrupting 3-dimensional structures and allosteric movements [51-53].
473 Although monovalent PMA cannot cross-link, it forms a bulky adduct with cysteines
474 (LaVoie, 2015), which may compromise protein folding. The proteases and chaperones
475 of the heat shock response degrade or repair misfolded proteins [54] and we found their
476 expression was increased by both mercurials (Figures 6 and S12 and Table S13). At 10
477 min, expression of protease genes *lon, clpXP* and *ftsH* had risen 4- to 6-fold with $HgCl_2$
478 and *lon* and *clpXP* were up 3-fold with PMA. $HgCl_2$ provoked up-regulation of all 12 heat
479 shock protein (HSP) and chaperone genes by 10 min, but only chaperones *clpB* and
480 *ybbN* mRNAs remained elevated at 30 min. Two other HSP genes, Hsp15 (*hslR*)

bioRxiv preprint doi: https://doi.org/10.1101/161646; this version posted July 10, 2017. The copyright holder for this preprint (which was not certified by peer review) is the author/funder, who has granted bioRxiv a license to display the preprint in perpetuity. It is made available under aCC-BY-NC-ND 4.0 International license.

involved in stalled ribosome recycling and Hsp31 (*hchA*) an amino acid deglycase, were further up-regulated by $HgCl_2$ at 60 min. In contrast, at 10 min PMA had up-regulated only five HSPs, increasing to six by 30 min and declining to three by 60 min. The *ibpA* and *ibpB* chaperone genes were among the most highly up-regulated genes for both $HgCl_2$ and PMA and persisted throughout recovery.

Of the 16 RNases and RNA processing enzymes only 3 increased: RNase R (3-fold for $HgCl_2$ and 5-fold for PMA) for both compounds during first 30 min; RNase III two-fold for PMA at 30 min; and RNase T two-fold for $HgCl_2$ at 60 min. The degradasome complex subunit genes (*rne, eno, rhlB, pnp, ppk*) [55] were all down-regulated for PMA during the first 30 min following exposure, except the helicase (*rhlB*), but only enolase was down-regulated for $HgCl_2$ (Figures 6 and S12 and Table S13). Expression of RNase II (*rnb)* was also down-regulated for both compounds, but with greater fold-changes observed for PMA. It is unclear what effect these changes in gene expression could have on RNA turnover and message decay rates while under mercury stress. As with the DNA metabolism genes, expression of the transcriptional apparatus shows that sufficient PMA was taken up to elicit both positive and negative responses distinct from $HgCl_2$.

ii. ENERGY PRODUCTION

(a) Electron transport chain

Expression of approximately 50% of all electron transport chain (ETC) genes was down-regulated during the first 30 min for $HgCl_2$ and PMA, with individual gene responses being very similar for both compounds (Figures 7 and S13 and Table S13).

bioRxiv preprint doi: https://doi.org/10.1101/161646; this version posted July 10, 2017. The copyright holder for this preprint (which was not certified by peer review) is the author/funder, who has granted bioRxiv a license to display the preprint in perpetuity. It is made available under aCC-BY-NC-ND 4.0 International license.

By 60 min, only 26% of these genes were down-regulated for $HgCl_2$, and none were down-regulated for PMA. Expression of NADH:unbiquinone oxidoreductase genes was down-regulated by both compounds, with 77% and 100% of these genes being down-regulated at 10 and 30 min, respectively. The ATP-synthase subunit genes were also strongly down-regulated by both mercurials at 10 and 30 min, but normal expression was restored at 60 min.

The *torCAD* locus that encodes the trimethylamine N-oxide anaerobic respiratory system was strongly up-regulated only by PMA exposure. This is likely an artifact of the dimethyl sulfoxide used to dissolve PMA, although the final DMSO concentration, 0.015% vol/vol (2.1 mM), was not expected to have any biological effect [56] and the anaerobic DMSO reductase genes (*dmsABC*) were down-regulated. It is unlikely that either the *tor* or *dms* responses significantly affect growth rate [57] or afford protection against either mercurial since over-expressed heme-dependent *torC* may be in the apoprotein form [58].

(b) Carbon metabolism

Expression of genes for carbon metabolism decreased generally, but there were more up-regulated genes in response to $HgCl_2$ and not all steps were affected equally by both mercurials (Figure S14). Expression of five genes of the pentose-phosphate pathway rose in at least one time point for $HgCl_2$, but only *pgl* increased for PMA at 10 min. The ribose-5-phosphate isomerase gene (*rpiB*), which is a backup enzyme for the gene product of *rpiA* [59], was up-regulated 40-fold for $HgCl_2$ at 10 min; although expression of *rpiA* did not differ from the unexposed cells for either mercurial at any

bioRxiv preprint doi: https://doi.org/10.1101/161646; this version posted July 10, 2017. The copyright holder for this preprint (which was not certified by peer review) is the author/funder, who has granted bioRxiv a license to display the preprint in perpetuity. It is made available under aCC-BY-NC-ND 4.0 International license.

time. Glycolysis responded similarly to both mercurials, with the greatest number of these genes being down-regulated at 30 min. The expression changes in TCA cycle genes were distinct for $HgCl_2$ and PMA; six genes were up-regulated in at least one time point for $HgCl_2$ and only one was up-regulated for PMA. Expression of several carbohydrate transport genes was down-regulated by both mercurials (Table S6).

(c) Nicotinamide adenine dinucleotide (NAD)

Expression of genes for nicotinamide adenine dinucleotide (NAD) and NAD-phosphate (NADP) synthesis and turnover pathways was repressed by mercury exposure (Figure S15). The biosynthesis genes were moderately down-regulated, with *nadB* being the only gene down for both mercurials at all times and *nadA* decreasing for $HgCl_2$ at 30 and 60 min and for PMA at 30 min. Expression of the *pncABC* salvage pathway did not change. The NAD reduction pathways were more affected than the NADP reduction pathways, with only *pgi* down for both mercurials and *edd* down only for $HgCl_2$. The transhydrogenase (*pntAB*) was down only for PMA at 10 and 30 min. Expression of other genes for NAD to NADH reduction in glycolysis and the TCA cycle were also down for both mercurials, which reflects the overall decrease in metabolism and energy production pathways.

Globally, redox metabolism declined immediately after exposure and normal gene expression levels were not restored until growth recovered to the pre-exposure rate. KEGG maps created using iPath [60] depict system-wide metabolism changes over time (Figures S16-S18 for $HgCl_2$ and Figures S19-S21 for PMA).

bioRxiv preprint doi: https://doi.org/10.1101/161646; this version posted July 10, 2017. The copyright holder for this preprint (which was not certified by peer review) is the author/funder, who has granted bioRxiv a license to display the preprint in perpetuity. It is made available under aCC-BY-NC-ND 4.0 International license.

iii. CENTRAL METABOLISM

(a) Amino acid metabolism and transport

The two mercurials had distinct effects on expression of genes for biosynthesis of amino acids (Figure 8 and S22). Since mercury targets cysteine thiol groups and will deplete the cellular reduced thiol pool, we expected an increase in cysteine and glutathione biosynthesis. Surprisingly, most genes for biosynthesis of these biothiols and for general sulfur metabolism were down-regulated or no different from the unexposed cells, with the exception of up-regulation of *cysE*, which is the first step in the biosynthesis pathway from serine.

Methionine biosynthesis gene expression increased for 7 genes with $HgCl_2$, but 11 genes were down-regulated with PMA, especially *metE* dropping 187-fold with PMA at 30 min (Figure 8 and S22). Expression of genes for histidine synthesis also responded differently to each mercurial, rising dramatically with $HgCl_2$ at 30 to 60 min. In contrast, all *his* genes expression dropped with PMA from 10 to 30 min. Genes for the synthesis of leucine, isoleucine, and valine had the opposite response, with most going down with $HgCl_2$ but increasing with PMA. Expression of other amino acid biosynthetic pathways was largely unchanged or declined with both mercurials. Branched-chain (*livKHMGF*), dipeptide (*dppABCDF*), and oligopeptide (*oppABCDF*) transporters were also down for both mercurials, with greater negative fold-changes for PMA (Table S5).

(b) Inorganic ion transport and metallochaperones

bioRxiv preprint doi: https://doi.org/10.1101/161646; this version posted July 10, 2017. The copyright holder for this preprint (which was not certified by peer review) is the author/funder, who has granted bioRxiv a license to display the preprint in perpetuity. It is made available under aCC-BY-NC-ND 4.0 International license.

572 Inorganic Hg(II) can displace beneficial thiophilic metals from their native binding
573 sites in proteins, potentially affecting transport and disrupting transition metal
574 homeostasis [23], leading to expression changes for non-ferrous metal cation and
575 oxoanion transporters (Figures 9 and S23 and Table S13), iron homeostasis (Figures
576 10 and S24 and Table S13) and metal-binding proteins and enzymes (Table S15).
577 Inorganic mercury exposure releases labile iron, which could itself increase
578 oxidative stress via Fenton chemistry under aerobic growth [23, 61]. Most iron uptake
579 pathways declined early for both mercurials, consistent with the observed increase in
580 expression of the Fur repressor. The cytochrome *c* maturation genes that transport
581 heme to the periplasm (*ccmABCDE*) were also down for both mercurials. The putative
582 ferrous iron and zinc efflux pump, *fieF* [62] increased 2-fold for $HgCl_2$ at 10 min only,
583 suggesting it may have a brief role in restoring one or both of these homeostases.
584 There are two iron-sulfur (Fe-S) cluster assembly pathways in *E. coli* [63, 64].
585 Expression of the primary Isc system (*iscRSUA*, *hscBA*, and *fdx*) increased strongly for
586 both mercurials, but with greater changes for $HgCl_2$ (Figures 10 and S24 and Table
587 S13). The secondary Fe-S cluster assembly system *sufABCDSE*, which activates under
588 oxidative stress or iron limiting conditions also increased greatly, but only for $HgCl_2$.
589 These transcriptional responses confirm and extend biochemical findings [23] that Fe-S
590 clusters are more vulnerable to inorganic mercury than to organomercurials and the cell
591 quickly tries to repair this damage.
592 Zinc uptake via expression of *zupT* increased modestly from 3 to 5-fold for both
593 mercurials during the first 30 minutes (Figures 9 and S23 and Table S13). In contrast,
594 expression of the P-type ATPase zinc efflux pump, *zntA* [65], increased 20- to 40-fold

bioRxiv preprint doi: https://doi.org/10.1101/161646; this version posted July 10, 2017. The copyright holder for this preprint (which was not certified by peer review) is the author/funder, who has granted bioRxiv a license to display the preprint in perpetuity. It is made available under aCC-BY-NC-ND 4.0 International license.

595 for both mercurials at 10 and 30 min and the periplasmic binding protein ZraP was up
596 throughout recovery. *E. coli* has two copper/silver efflux systems, Cue and Cus [66].
597 Surprisingly, the Cus system genes (*cusRS, cusCFBA)* primarily used under anaerobic
598 conditions were among the most down-regulated genes under PMA exposure. The Cue
599 system consists of the multi-copper oxidase, CueO, and a P-type ATPase, CopA, both
600 regulated by the MerR homolog, CueR. Both *cueO* and *copA* were up over 20-fold with
601 $HgCl_2$ at 10 and 30 min, but only 5-fold with PMA briefly at 10 min. The nickel uptake
602 system [67] (*nikABCDER*) was also very strongly down-regulated under PMA exposure
603 conditions through all times although expression of repressor NikR was unchanged,
604 except for a 3-fold increase with $HgCl_2$ at 10 min. Expression of the nickel and cobalt
605 efflux gene, *rcnA*, increased with $HgCl_2$ or PMA. Manganese (*mntH*), and magnesium
606 (*mgtA, corA*) uptake genes increased with both mercurials.
607 Inorganic anions used by *E. coli* include phosphate, sulfate, and molybdate and
608 genes for defense against arsenate, a phosphate mimic (Figures 9 and S23 and Table
609 S13). Expression of the ABC phosphate transport system (*pstSCAB*) genes increased
610 greatly for both mercurials, with PMA-provoked changes up to 165-fold for the
611 phosphate binding protein, *pstS*. The two-component phosphate regulatory system,
612 PhoBR increased 22-fold with $HgCl_2$ and 105-fold with PMA for *phoB*. Sulfate and
613 thiosulfate uptake by the ABC transporter (*cysPUWA*) decreased strongly with $HgCl_2$ at
614 30 min and PMA at 10 and 30 min. Expression of molybdate uptake (*modABC*)
615 increased with PMA during the first 30 min but only at 10 min with $HgCl_2$. The arsenate
616 resistance operon cannot effect Hg(II) resistance, but was highly induced by both

bioRxiv preprint doi: https://doi.org/10.1101/161646; this version posted July 10, 2017. The copyright holder for this preprint (which was not certified by peer review) is the author/funder, who has granted bioRxiv a license to display the preprint in perpetuity. It is made available under aCC-BY-NC-ND 4.0 International license.

617 mercurials, perhaps through interacting with the three-cysteine metal-binding site of the
618 ArsR repressor [68].
619
620 iv. SURFACE FUNCTIONS
621 *(a) Cell wall biogenesis, porins, lps, efflux systems, and electrolyte balance*
622 The transcriptional response of peptidoglycan, membrane biosynthesis, and cell
623 division genes was similar for both mercurials (Figure S25 and Table S13). Expression
624 increased for roughly 20% of lipid biosynthesis genes, including those for cardiolipin,
625 and expression decreased for 20-30% of other lipid-related genes. Transcription of
626 genes for murein synthesis (*murCDEFGIJ*) in particular declined for both mercurials
627 during the first 30 min.
628 *E. coli* encodes several antibiotic resistance efflux systems that are up-regulated
629 by mercury exposure (Figures 11 and S26 and Table S13). The multiple antibiotic
630 resistance locus (*marRAB*), which increases drug efflux and also limits passive uptake
631 by decreasing porin expression [69], was strongly up-regulated by both mercurials with
632 greater changes observed for PMA. Though expression of some porin genes (*ompC,*
633 *ompF, ompT, ompW*) was repressed, three non-specific porins (*ompG, ompL, ompN*)
634 were up-regulated only by PMA. Genes from several TolC-dependent antibiotic efflux
635 systems were up-regulated by both mercurials as well, including *acrEF, emrD, emrKY,*
636 and several *mdt* genes [70]. $HgCl_2$ exposure alone also up-regulated two-component
637 sensor genes (*phoQP* at 10 min and *basSR* at 60 min) that regulate genes involved in
638 modification of the cell surface and increase polymyxin resistance [71], but most of
639 these genes were down-regulated or unchanged for PMA.

bioRxiv preprint doi: https://doi.org/10.1101/161646; this version posted July 10, 2017. The copyright holder for this preprint (which was not certified by peer review) is the author/funder, who has granted bioRxiv a license to display the preprint in perpetuity. It is made available under aCC-BY-NC-ND 4.0 International license.

The response to osmotic stress and maintenance of electrolyte balance are important membrane functions requiring adaptation in dynamic natural environments. During $HgCl_2$ exposure the expression of the sodium antiporter, NhaA, increased 4-fold at 10 min and the calcium/potassium antiporter, ChaA, was up 3-fold at 10 and 30 min (Figures 9 and S23 and Table S13). In contrast, expression of genes for transport of the major electrolyte, potassium, changed only modestly in some subunits of the *kdp, kef*, and *trk* systems, without an obvious response pattern. However, transcription of genes for defense against osmotic stress was uniformly up-regulated; betaine genes (*betABIT and proP*), *osmBCEFY, and* mechanosensitive channel proteins (*mscL* and *mscS*) increased for both mercurials, as did a putative osmoprotectant ABC permease (yehYXW) [72] only with $HgCl_2$ at 30 and 60 min (Table S5).

(b) Motility and biofilm

Nearly all flagellar component genes were strongly down-regulated for both mercurials, with negative changes being much greater for PMA than for $HgCl_2$ exposure (Figures 12 and S27). Only PMA increased expression of fimbriae and curli fiber genes, which alter motility and increase adhesion (Figure 13 and S28) [73]. Fifteen genes up-regulated by PMA exposure were annotated as homologs of FimA, but with unknown function. FimA is the major structural component of fimbriae, but these genes may serve other functions. Motility genes whose expression dropped remained low until 60 min, indicating that the structurally and energetically intensive motility systems are very slow to recover.

bioRxiv preprint doi: https://doi.org/10.1101/161646; this version posted July 10, 2017. The copyright holder for this preprint (which was not certified by peer review) is the author/funder, who has granted bioRxiv a license to display the preprint in perpetuity. It is made available under aCC-BY-NC-ND 4.0 International license.

$HgCl_2$ and PMA also provoked expression of several biofilm-related genes (Figures 13 and S28 and Table S13). The *bhsA* and *bdcA* loci were among the most highly up-regulated genes during $HgCl_2$ exposure, with much higher fold-changes than observed for PMA (Tables 2 and 3). Neither gene is well characterized, but independently each has been found to decrease biofilm formation and increase resistance to external stressors [74, 75]. Only PMA increased expression of genes for poly-β-1,6-N-acetyl-glucosamine (PGA) polysaccharide production [76] and biofilm related genes, *ycgZ, ymgA, ariA, ymgC* [77]. Thus, PMA elicits a broader response that potentially alters the cell surface and may increase adhesion and biofilm formation; in contrast $HgCl_2$ only inhibits motility and does not activate adhesion pathways. It is possible that some changes observed for motility and biofilm related genes following PMA-exposure are an artifact of the DMSO, but other studies suggest that solvent would have no effect or that much higher concentrations than used here would be required to induce these changes [56, 78].

v. STRESS RESPONSES

(a) Oxidative stress response and repair

There are two oxidative stress response pathways in *E. coli*, the *oxyRS* and *soxRS* regulons [61, 79]. OxyR, a LysR-family transcriptional regulator, uses a cysteine-pair to sense oxidative damage and regulates 49 genes when oxidized [80]. $HgCl_2$ exposure increased expression of 22 OxyR regulon genes at 10 min; these then declined to 13 genes by 60 min (Table S16). In contrast, PMA provoked expression of 16 OxyR regulon genes at 10 and 30 min, but none at 60 min. *OxyS*, a small non-

bioRxiv preprint doi: https://doi.org/10.1101/161646; this version posted July 10, 2017. The copyright holder for this preprint (which was not certified by peer review) is the author/funder, who has granted bioRxiv a license to display the preprint in perpetuity. It is made available under aCC-BY-NC-ND 4.0 International license.

685 coding RNA regulated by OxyR, represses *rpoS*, *fhlACD* and other genes to prevent
686 redundant induction of stress response genes [81]. The *oxyS* gene was among the most
687 highly expressed genes with over a 1,000 fold-change with $HgCl_2$ at 10 and 30 min, and
688 a more modest change of 10-fold at 10 min and 6 fold at 30 min with PMA.

689 The SoxRS regulon is the other oxidative stress response system in *E. coli*.
690 SoxR, a MerR-family repressor-activator, uses the oxidation state of 2Fe-2S clusters to
691 respond to superoxide (O_2^-) stress and induce transcription of *SoxS* [82-85], which then
692 transcriptionally regulates 53 genes [79, 86] (Table S16). $HgCl_2$ or PMA exposure up-
693 regulated 22 or 25 genes, respectively, at 10 min and these had declined to 13 or 0
694 genes, respectively by 60 min.

695 Key genes in these oxidative stress regulons differentially expressed upon
696 mercury exposure include the ROS scavengers: catalase (*katG*), alkyl hydroperoxide
697 reductase (*ahpCF*), and superoxide dismutase (*sodA*) (Figures 14 and S29 and Table
698 S13). Thiol homeostasis genes included *gor*, *grxA,* and *trxC* (Figures 14 and S29 and
699 Table S13). Iron homeostasis and the Fe-S cluster assembly and repair genes (*fur, dps,*
700 *fldA, fpr, hemH, sufABCDES,* and *yggX*) were also up-regulated. PMA provoked
701 comparatively lower fold-changes than $HgCl_2$ for *grxA, trxC, ahpC, dps, fldA, hemH, and*
702 *yggx*. The manganese uptake protein, *mntH*, plays an important role in ROS resistance
703 [87] and was up for both mercurials. Oxidation-resistant dehydratase isozymes, *acnA*
704 and *fumC* [88, 89] also increased, but only for $HgCl_2$ exposure. Thus, both mercurials
705 triggered the Oxy and Sox oxidative stress responses, but $HgCl_2$ elicited greater fold-
706 changes overall than PMA compared to unexposed cells.

bioRxiv preprint doi: https://doi.org/10.1101/161646; this version posted July 10, 2017. The copyright holder for this preprint (which was not certified by peer review) is the author/funder, who has granted bioRxiv a license to display the preprint in perpetuity. It is made available under aCC-BY-NC-ND 4.0 International license.

Because mercury poisons the cellular thiol pool [23], we expected that regulation of redox homeostasis proteins such as glutaredoxins, thioredoxins and glutathione-related genes would respond to mercury exposure (Figure 14 and S29). Glutaredoxin 1 (*grxA*) expression was up for both mercurials with a greater fold-change for $HgCl_2$, but glutaredoxin 2 (*grxB*) was down for both mercurials, while glutaredoxin 3 (*grxC*) and glutaredoxin 4 (*grxD*) were up only for PMA. Thioredoxin reductase (*trxB*) increased two-fold with PMA (30 min only), but was up with $HgCl_2$ 8-fold (10 min) and 4-fold (30 min). Thioredoxin 1 (*trxA*) expression increased two-fold only with PMA (10 min), in contrast to thioredoxin 2 (*trxC*), which was up for both mercurials, but much higher with $HgCl_2$ than with PMA. However, the thiol peroxidase (*tpx*) was up modestly for PMA, but did not change for $HgCl_2$. Thus, while each mercurial stresses the cell to maintain redox homeostasis, a greater burden is created by $HgCl_2$ exposure.

Glutathione (GSH) serves as the cell's redox buffer and as a scavenger of mercurials (Figures 14 and S29 and Table S13). Surprisingly, expression of GSH biosynthesis and utilization genes increased only modestly. The γ-glutamyltranspeptidase (*ggt*) increased late (60 min) by 4-fold only with $HgCl_2$. GSH synthase (*gshA*) did not change and *gshB* was up 2-3 fold for both mercurials only at 10 min. The GSH importer (*gsiABCD*) may be a salvage pathway to recover GSH and cysteine leaked into the periplasm by CydCD [90, 91], but it was down-regulated by $HgCl_2$ or PMA through 30 min. The GSH reductase (*gor*) increased only with $HgCl_2$ at 10 min and several GSH S-transferase genes involved in detoxification [92] (*gstA, gstB, yfcF, yqjG, yibF, yncG*) increased with both mercurials. Since all of these proteins have Hg(II)-vulnerable cysteines in their active sites, it is surprising that neither Hg(II) nor

bioRxiv preprint doi: https://doi.org/10.1101/161646; this version posted July 10, 2017. The copyright holder for this preprint (which was not certified by peer review) is the author/funder, who has granted bioRxiv a license to display the preprint in perpetuity. It is made available under aCC-BY-NC-ND 4.0 International license.

PMA-challenged cells provoked increased expression and suggests that their normal mRNA levels are sufficient to replenish them.

(b). Genes with delayed up-regulation

Genes unchanged at 10 min but differentially expressed at both 30 and 60 min or 60 min alone may be those needed as cells transition out of stasis and towards normal growth (Table S17). For $HgCl_2$ exposure, 95 genes were up-regulated and 140 genes were down-regulated that display this delayed response pattern. Approximately half of the up-regulated genes are involved in energy production, transport and metabolism pathways based on COG annotations. Roughly 45% of these delayed $HgCl_2$ provoked, up-regulated genes are the same as genes that were differentially expressed during the first 30 min of PMA exposure. This overlap is consistent with slower recovery of growth in $HgCl_2$ exposed cells and that some of the same pathways are used for recovery by both compounds. In contrast, for the more quickly recovering PMA exposure, of the genes that showed no change at 10 min only six were up-regulated at 60 min (Table S17). Only two of these delayed-response genes for PMA exposure overlapped with up-regulated genes for $HgCl_2$ exposure.

DISCUSSION

Mercury is a ubiquitous toxicant that serves no biologically beneficial role. Exposure to any form of mercury negatively impacts the health of organisms from microbes to humans. The biological effects of different forms of mercury are often conflated and methylmercury is assumed to be the most toxic form. However, the

bioRxiv preprint doi: https://doi.org/10.1101/161646; this version posted July 10, 2017. The copyright holder for this preprint (which was not certified by peer review) is the author/funder, who has granted bioRxiv a license to display the preprint in perpetuity. It is made available under aCC-BY-NC-ND 4.0 International license.

753 systemic biochemical and molecular differences between inorganic and organic mercury
754 compounds have yet to be well characterized from exposure through recovery in a
755 single model system.
756
757 ***BULK DIFFERENTIAL EFFECTS ON GROWTH AND GENE EXPRESSION***
758 The sub-acute mercury exposure conditions used in this study were chosen by
759 identifying a mercury concentration high enough to stop cells from doubling, but low
760 enough to allow restoration of the pre-exposure growth rate within one-hour (~1
761 generation period) after exposure (Figure 1a). Concentrations below 3 μM of either
762 compound did not consistently inhibit growth and higher concentrations of $HgCl_2$ did not
763 allow recovery within the desired time frame. Three micromolar Hg is well within the
764 range that bacteria can experience chronically from dental amalgam fillings [93] and in
765 highly contaminated environments, such as artisanal gold mining operations [8].
766 Mercury in tuna is 0.386 ppm compared to the proxy organomercurial, PMA, used here
767 at 3 μM or 0.6 ppm [94].
768 PMA-exposed cells recovered exponential growth faster (Figure 1) than those
769 with equimolar exposure to $HgCl_2$, perhaps owing to lower uptake of PMA (Table S2).
770 However, PMA-exposed cells differentially expressed more genes than $HgCl_2$ exposed
771 cells during the first 30 min of exposure (Figure 1b). These results agree with
772 observations in *C. elegans,* where MeHg exposure resulted in four times more DEGs
773 than did $HgCl_2$ for all concentrations tested [95]. However, in contrast to *E. coli,* whose
774 growth was inhibited more by inorganic $HgCl_2$, in *C. elegans* the effective toxic
775 concentration of methylmercuric chloride was lower than for $HgCl_2$ [95].

bioRxiv preprint doi: https://doi.org/10.1101/161646; this version posted July 10, 2017. The copyright holder for this preprint (which was not certified by peer review) is the author/funder, who has granted bioRxiv a license to display the preprint in perpetuity. It is made available under aCC-BY-NC-ND 4.0 International license.

We found that most DEGs peaked at 10 min after exposure for both compounds with $HgCl_2$ provoking more down-regulation and PMA yielding more up-regulated genes throughout the exposure period (Figure 1b). Even though the optical density (OD) of the $HgCl_2$ exposed culture showed no growth recovery from 10 min to 30 min, DEGs decreased by 22%, while PMA-exposed cells over the same period had a moderate increase in OD, but only an 8% decrease in DEGs (Figure 1). In contrast in a eukaryotic system, the livers of $HgCl_2$ exposed zebrafish continuously increased in DEGs throughout the observed 96 hour exposure period as mercury accumulated in their cells [96].

In *E. coli,* during the first 30 min post-exposure, 50-70% of both up- and down-regulated genes were the same for both compounds (Figure 2), but at the level of individual genes there were both qualitative and quantitative differences in expression (Table S5), consistent with idiosyncratic transcriptional responses to each compound. The nematode *C. elegans* also manifested distinct and even some opposite transcriptional responses to inorganic and organic mercury exposure in a single end-point microarray experiment [24].

As there are not yet other studies of the transcriptional response of a bacterium to mercury exposure, on the basis of the findings in eukaryotes and our proteomic work [23] we have organized our observations here into those we had expected and those we did not expect from any yet published work.

EXPECTED AND UNEXPECTED GENE-SPECIFIC CHANGES

Expected transcriptional changes:

bioRxiv preprint doi: https://doi.org/10.1101/161646; this version posted July 10, 2017. The copyright holder for this preprint (which was not certified by peer review) is the author/funder, who has granted bioRxiv a license to display the preprint in perpetuity. It is made available under aCC-BY-NC-ND 4.0 International license.

(a) Thiol homeostasis. The millimolar cytosolic pool of glutathione (GSH) can sequester mercurials and thereby protect protein thiols from binding strongly to these soft metal toxicants. However, if the GSH pool becomes depleted by mercury complexation, the cell loses this primary defense mechanism. Since proteins of the stress response and repair pathways all contain active site thiols, often as part of Hg(II)-vulnerable Fe-S centers, it is not obvious how a cell that has lost much of its available thiols to Hg(II) chelation can restore its metabolism. Given this, we expected cysteine and glutathione biosynthesis pathways to be up-regulated. However, cysteine biosynthesis was down (Figures 8 and S22 and Table S13) and GSH biosynthesis was mostly unchanged (Figures 14 and S29 and Table S13) for both compounds, in contrast to the eukaryotic response to mercury [96-98] and H_2O_2 exposure [99], which increase GSH and metallothionein production. However, although thiol biosynthesis did not increase, genes involved in maintaining cellular thiol homeostasis did increase (Figures 14 and S29 and Table S13); thioredoxin (*trxC*) and glutaredoxin (*grxA*) were among the most highly up-regulated genes with $HgCl_2$ and PMA exposure. Others have also found in *E. coli* that glutathione reductase increased with $HgCl_2$ and both compounds increased expression of glutathione oxidoreductase and S-transferase genes, which protect against oxidative stress and xenobiotics [100].

(b) Iron homeostasis. We also expected inorganic mercury to disrupt iron-sulfur clusters with consequent effects on Fe homeostasis generally [23, 101]. Iron uptake was down-regulated with both mercurials, consistent with excess intracellular free Fe(II) and general oxidative stress, but expression of the uptake repressor (*fur*) was only up for

bioRxiv preprint doi: https://doi.org/10.1101/161646; this version posted July 10, 2017. The copyright holder for this preprint (which was not certified by peer review) is the author/funder, who has granted bioRxiv a license to display the preprint in perpetuity. It is made available under aCC-BY-NC-ND 4.0 International license.

822 $HgCl_2$ (Figure 10 and S24). *Fur* expression is activated by either OxyR or SoxS [99,
823 102] and Fur represses Fe uptake pathways with ferrous iron as a co-repressor [103].
824 Fur can also bind other divalent metals [104], so Hg(II)-Fur might mimic Fe-Fur as an
825 iron uptake repressor under these conditions to limit Fenton-mediated damage from
826 excess iron. Although both mercurials increased expression of the primary Fe-S cluster
827 assembly and repair system (*isc*), only $HgCl_2$ induced the secondary system (*suf*),
828 which is normally induced under oxidative stress or iron limiting conditions [63, 105]
829 (Figures 10 and S24 and Table S13). Also, only $HgCl_2$ exposure increased expression
830 of iron storage proteins: ferritin, bacterioferritin, and Dps (Figure 10 and S24). The DNA
831 binding protein Dps which binds free iron to protect DNA from ROS damage [106] was
832 one of the most highly up-regulated genes with $HgCl_2$ exposure (Table 1).
833
834 *(c)* Oxidative stress response. The known close link between iron homeostasis and
835 oxidative stress [61] explains the high fold-changes upon $HgCl_2$ exposure in genes that
836 respond to oxidative stress (Table S16) and echoes mercury's long known stimulation of
837 oxidative damage in rat kidney mitochondria [107]. The small non-coding RNA *oxyS*
838 was the second most highly up-regulated gene upon $HgCl_2$ exposure with differential
839 expression more than 100-fold greater than observed for PMA (Table 1). The ROS
840 scavenger *ahpF* was also highly up-regulated, along with *katG* (early) and *sodA*
841 (delayed) but only for $HgCl_2$ (Figures 14 and S29 and Table S16). Other ROS resistant
842 enzymes, aconitase A [89] and fumarase C [108] (Table S16) also increased only for
843 $HgCl_2$, as did the manganese-dependent alternative ribonucleotide reductase genes
844 (*nrdHIEF*) [109]. The glutaredoxin-like protein that functions like thioredoxin, *nrdH* [110],

bioRxiv preprint doi: https://doi.org/10.1101/161646; this version posted July 10, 2017. The copyright holder for this preprint (which was not certified by peer review) is the author/funder, who has granted bioRxiv a license to display the preprint in perpetuity. It is made available under aCC-BY-NC-ND 4.0 International license.

was highly up-regulated by $HgCl_2$ and might support other thioredoxin and glutaredoxin proteins. These striking differences in gene expression illuminate how *E. coli* modulates expression of specific genes not only to deal with compromised function of specific $HgCl_2$ modified proteins, but also to manage the consequent cascade of reactive oxygen species.

(d) Heat shock response. Mercurials bound to protein cysteines could disrupt protein folding, subunit assembly, and allosteric movements [52, 111] and inorganic mercury can crosslink neighboring cysteines leading to aggregation [51]. Increased expression of heat shock response genes was expected as a consequence of such anticipated protein misfolding problems [112]. Indeed, expression of heat shock chaperonins and protease genes increased for both mercurials, with more genes up early in response to $HgCl_2$ than to PMA (Figures 6 and S12 and Table S13). Genes for the small chaperone-like proteins, *ibpA* and *ibpB*, were among the most highly increased for both compounds, especially for $HgCl_2$ (Table 1), consistent with their role in aiding Lon protease in the degradation of misfolded proteins [113-115].

(e) Translational apparatus. Thiophilic Cd^{2+} exposure in *E. coli* has been shown to decrease expression of ribosomal proteins [116]. In our proteomics work (Zink et al. in preparation) we observed fourteen r-proteins (7 for each ribosomal subunit) that formed stable adducts with either PMA or Hg(II), so it was reasonable to expect this to be reflected in transcription of r-proteins. Indeed, $HgCl_2$ exposure repressed expression of up to 83% of r-protein genes at 10 min and 74% at 30 min (Figure 5, S11, and Table

bioRxiv preprint doi: https://doi.org/10.1101/161646; this version posted July 10, 2017. The copyright holder for this preprint (which was not certified by peer review) is the author/funder, who has granted bioRxiv a license to display the preprint in perpetuity. It is made available under aCC-BY-NC-ND 4.0 International license.

868 S14), whereas PMA only briefly repressed expression of 41% of r-proteins at 30 min.
869 Divalent inorganic mercury's ability to cross-link proteins may interfere with ribosome
870 assembly resulting in translational feedback and repression of r-proteins transcription.
871 Disruption of ribosome assembly could also contribute to the slower recovery of growth
872 after inorganic Hg(II) exposure.
873
874 *(f)* Energy production. The dependence of most energy production pathways on redox-
875 active transition metals and redox-active sulfur compounds made them obvious targets
876 of mercurial disruption, e.g. three ATP-synthase subunits form stable adducts after in
877 vivo exposure to Hg(II) or PMA (Zink et al. in preparation). Intriguingly, expression of
878 genes within this functional category was largely down-regulated early in exposure, with
879 all nine ATPase subunits down for $HgCl_2$ (10 min) and eight down for PMA (30 min)
880 (Figure 7 and S13). Although others have found that Cd exposure in *E. coli* repressed
881 aerobic energy metabolism genes and induced anaerobic pathways [116], we found that
882 both aerobic and anaerobic energy metabolism were repressed by $HgCl_2$ and PMA.
883 Even though expression of the oxygen-sensing *fnr* [117] and *aer* [118, 119] activators of
884 the anaerobic shift were moderately up for PMA and unchanged for $HgCl_2$ (Table S5).
885 Similarly, glucose metabolism genes were also predominantly down during early
886 periods for both compounds, especially with PMA exposure (Figure S14). Thus, with
887 severely compromised energy production systems, it is not surprising that amino acid,
888 carbohydrate and nucleotide metabolism genes, and the energy-dependent transport of
889 these molecules (Figure 3 and Table S6), are also largely depressed initially.
890

bioRxiv preprint doi: https://doi.org/10.1101/161646; this version posted July 10, 2017. The copyright holder for this preprint (which was not certified by peer review) is the author/funder, who has granted bioRxiv a license to display the preprint in perpetuity. It is made available under aCC-BY-NC-ND 4.0 International license.

(g) Homeostases of non-ferrous metals. We expected mercurials to disrupt electrolyte balance [23], but expression of the potassium efflux pumps' subunit genes (*kcpABC, kefBC, and trkAGH*) were not uniformly up-regulated, although the need to restore the pH balance was indicated by briefly increased expression of the H^+/Na^+ antiporter (*nhaA*) for both compounds (Figures 9, S23 and Table S5). It may be that normal levels of the proteins involved in maintaining cellular electrolyte balance are sufficient to respond to mercury exposure and a significant change in transcriptional expression is not required for these genes.

Mercury is also expected to disrupt non-ferrous metal homeostasis because it can displace other metals, such as zinc and copper, as enzyme cofactors [120, 121]. Expression of metal uptake genes decreased and of metal efflux genes increased for zinc, copper, nickel and cobalt, with generally greater fold-changes for $HgCl_2$. Zinc efflux by ZntA is regulated by the MerR homolog ZntR, which can respond to Hg(II) [122], but has not been shown to confer resistance to Hg(II) exposure. Indeed, *in vitro* the ATPase activity of the ZntA efflux pump is stimulated by Hg-thiolate complexes [65, 123]. This could be a possible source for the decline in inorganic Hg content observed over time (Table S2) once bound by glutathione or cysteine, but would not explain the increase at 60 min or decline in PMA, unless other efflux systems such as antibiotic resistance systems are effective as well. Manganese may protect iron metalloenzymes under oxidative stress conditions [87] and Mn uptake by *mntH,* as part of the OxyR regulon, was correspondingly up-regulated for both compounds in response to mercury-induced oxidative stress.

bioRxiv preprint doi: https://doi.org/10.1101/161646; this version posted July 10, 2017. The copyright holder for this preprint (which was not certified by peer review) is the author/funder, who has granted bioRxiv a license to display the preprint in perpetuity. It is made available under aCC-BY-NC-ND 4.0 International license.

Unexpected transcriptional changes:

(a) Motility and chemotaxis. Energetically costly flagellar motility and chemotaxis were strongly down-regulated by both mercurials and were among the slowest to recover normal transcription levels (Figures 12 and S27 and Table S13). Motility gene expression is regulated by σ^{28} (*fliA*) and FlhDC [124] and the expression of these two regulatory genes declined with $HgCl_2$ but was unchanged with PMA. Repression of motility may occur through sigma factor competition for binding to RNAP between σ^{28} and increased expression of σ^{S} [125] and/or through repression of the flagellar transcriptional activator FlhDC by increased expression of the small ncRNAs *oxyS* and *gadY* [126]. Interestingly, $HgCl_2$ exposure impaired locomotion in *C. elegans* [24], although through a very different mechanism of motility from *E. coli*.

(b) Surface appendages and biofilm synthesis. Surprisingly, there were large increases in expression of genes involved in biofilm formation and adhesion or dispersal (Figures 13 and S28 and Tables S13). Expression of *bhsA* and *bdcA,* which function in biofilm dispersal or reduced biofilm formation [74, 75]*,* were the first and third, respectively, most up-regulated genes by $HgCl_2$ (Table 1) and were also up for PMA, but with much lower fold-changes (Table 2). Expression of *bhsA* is also up-regulated by other diverse stressors and may decrease cell permeability [75, 127]. PMA exposure especially increased expression of genes for the polysaccharide PGA, which aids in adhesion in biofilm formation [76], and other biofilm formation (*ycgZ, ymgA, ariA, ymgC*) genes [77] (Figures 13 and S28 and Table S13).

bioRxiv preprint doi: https://doi.org/10.1101/161646; this version posted July 10, 2017. The copyright holder for this preprint (which was not certified by peer review) is the author/funder, who has granted bioRxiv a license to display the preprint in perpetuity. It is made available under aCC-BY-NC-ND 4.0 International license.

936 Expression of fimbriae (*fim)* and curli fibers (*csg*), important for adhesion in
937 biofilm formation [73] were also up-regulated only by PMA (Figure 13 and S28), as were
938 15 of 22 FimA homologs of unknown function. Outer membrane vesicle formation
939 (OMVs) could also play a role in detoxification, since an increase in formation of these
940 vesicles has been associated with heat shock, oxidative stress response, and biofilm
941 formation [128], which are responses up-regulated to varying degrees by both
942 mercurials. These are distinct differences between PMA and $HgCl_2$ response. PMA
943 provocation of biofilm formation and adhesion genes might be an artifact of its DMSO
944 solvent, but it is not obvious why $HgCl_2$ induces such high increases in biofilm dispersal
945 genes.
946
947 *(c)* Phosphate metabolism. Phosphate uptake genes were among the most highly up-
948 regulated genes for PMA exposure (Figure 9, S23, and Table 2). The PhoBR two-
949 component system controls expression of phosphate transport genes, as well as some
950 genes that increase virulence including those for fimbriae and biofilm formation [129].
951 Since expression of PhoBR and its regulon increases under phosphate limiting
952 conditions [130], it may be that PMA inhibits phosphate uptake by an unknown
953 mechanism, possibly through direct interaction with highly up-regulated PstS or this
954 could be an artifact of DMSO.
955
956 *(d)* Amino acid biosynthesis. Expression of most amino acid pathways was turned down
957 by both compounds, but a few responded uniquely to each mercurial (Figures 8 and
958 S22 and Table S13). Since methionine auxotrophy occurs under oxidative stress due to

bioRxiv preprint doi: https://doi.org/10.1101/161646; this version posted July 10, 2017. The copyright holder for this preprint (which was not certified by peer review) is the author/funder, who has granted bioRxiv a license to display the preprint in perpetuity. It is made available under aCC-BY-NC-ND 4.0 International license.

959 ROS susceptibility of methionine synthase (MetE) [131], expression of methionine
960 biosynthesis genes may have been increased by $HgCl_2$, which provoked a stronger
961 oxidative stress response than PMA. However, since PMA did provoke some oxidative
962 stress response, it is curious that Met operon expression was strongly down under PMA
963 exposure. Next to its affinity for cysteine sulfur, Hg(II) binds the imino nitrogen of
964 histidine very strongly [132], so it was intriguing that histidine biosynthesis genes were
965 also up-regulated by $HgCl_2$ but down-regulated by PMA. It remains unclear how these
966 differences or the opposite responses for leucine, isoleucine and valine biosynthesis
967 help the cell survive mercurial exposure.
968
969 *(e)* Miscellaneous genes. Multiple antibiotic efflux systems and polymyxin resistance
970 surface modifications were up-regulated by $HgCl_2$ exposure, and even more so by PMA
971 (Figures 11 and S26 and Table S13). Chronic mercury exposure contributes to the
972 spread of multiple antibiotic resistant bacteria through co-selection of plasmid-borne
973 antibiotic and mercury resistance genes [133, 134]. Increased expression of antibiotic
974 resistance and surface components hint that low-level mercury exposure could prime
975 cells for increased antibiotic resistance. However, the ubiquity of plasmid- and
976 transposon-borne Hg resistance loci suggests that expression of these chromosomal
977 genes offers insufficient protection against the antibiotic or mercurial levels encountered
978 in clinical practice.
979 A handful of vestigial e14 or CPS-53 prophage genes were up-regulated by
980 $HgCl_2$ (Table 1) or PMA (Table S5), respectively. Some are known to increase

bioRxiv preprint doi: https://doi.org/10.1101/161646; this version posted July 10, 2017. The copyright holder for this preprint (which was not certified by peer review) is the author/funder, who has granted bioRxiv a license to display the preprint in perpetuity. It is made available under aCC-BY-NC-ND 4.0 International license.

resistance to osmotic, oxidative, and acid stressors [135, 136], but their roles and mechanisms have not been well defined.

(f) Differential expression of genes required for the same functional protein complex. In many instances we observed that transcripts for subunits of the same enzyme, protein complex, or component of a tightly articulated pathway were differentially expressed. In some cases these proteins lie in distinct transcripts, which may experience different turnover rates and in other cases the differences could be due to transcriptional polarity. We have chosen not to deal explicitly with such paradoxes in this work, which is sufficiently complex as it is, but will address them in future work.

CONCLUSIONS

The effects of mercury exposure in multicellular organisms have long been studied at the physiological level but a global, fine grained understanding of the differences in the precise biochemical sequelae of inorganic and organic mercury exposure has been lacking. This study is the first to examine not only the transcriptional response differences between inorganic mercury ($HgCl_2$) and an organomercurial (phenylmercuric acetate) in a model microorganism, but also first to examine longitudinally how the cell recovers from these chemically distinct compounds. Taken together with global identification of vulnerable protein targets (Zink et al. in preparation) and of damage to thiol and metal ion homeostasis upon acute mercurial exposure [23], the current work provides a quantitative systems-level description of the effects of *in vivo* mercury exposure in *E. coli*. What was striking and most challenging with this study

bioRxiv preprint doi: https://doi.org/10.1101/161646; this version posted July 10, 2017. The copyright holder for this preprint (which was not certified by peer review) is the author/funder, who has granted bioRxiv a license to display the preprint in perpetuity. It is made available under aCC-BY-NC-ND 4.0 International license.

was the breadth and diversity of the systems whose expression was affected by these two chemically distinct mercurials. Sub-acute exposure influenced expression of ~45% of all genes with many distinct responses for each compound, reflecting differential biochemical damage by each mercurial and the corresponding resources available for repair. Energy production, intermediary metabolism and most uptake pathways were initially down-regulated by both mercurials, but nearly all stress response systems were up-regulated early by at least one compound. These results echo the wide functional variety of proteins stably modified by these mercurials owing to the widespread occurrence of cysteines found in nearly all *E. coli* proteins. Microbiome studies are rapidly unveiling the importance of commensal bacteria to the health of all higher organisms. Our findings in this model commensal organism provide insights into how chronic mercury exposure might affect such complex microbial communities and, consequently, the health of the host. This work also serves as a foundation for studies now underway of how the widely found mobile Hg resistance (*mer*) locus assists the cell in recovery from Hg exposure.

LIST OF ABBREVIATIONS:

Hg = mercury

$HgCl_2$ = mercuric chloride

PMA = phenylmercuric acetate

PhHg = phenylmercury

DMSO = dimethyl sulfoxide

LB = Luria-Bertani medium

bioRxiv preprint doi: https://doi.org/10.1101/161646; this version posted July 10, 2017. The copyright holder for this preprint (which was not certified by peer review) is the author/funder, who has granted bioRxiv a license to display the preprint in perpetuity. It is made available under aCC-BY-NC-ND 4.0 International license.

NM3 = Neidhardt MOPS minimal medium

NGS = next generation sequencing

DEGs = differentially expressed genes

CVAA = cold vapor atomic absorption

GSH = glutathione

Cys = cysteine

MDR = multidrug resistance

ncRNA = non-coding RNA

COGs = clusters of orthologous groups

GOFs = gene-ontology functions

RNAP = RNA polymerase

HSP = heat shock protein

ETC = electron transport chain

PGA = poly-β-1,6-N-acetyl-glucosamine

DECLARATIONS

Ethics approval and consent to participate: Not applicable

Consent for publication: Not applicable

Availability of data and materials: The tabulated datasets supporting the conclusions of this article are included as additional files. The read counts and raw sequence data (.fastq) are stored in the Gene Expression Omnibus database (http://www.ncbi.nlm.nih.gov/geo/) with accession ID: GSE95575; they are available to

bioRxiv preprint doi: https://doi.org/10.1101/161646; this version posted July 10, 2017. The copyright holder for this preprint (which was not certified by peer review) is the author/funder, who has granted bioRxiv a license to display the preprint in perpetuity. It is made available under aCC-BY-NC-ND 4.0 International license.

reviewers upon request and will be open to the public when the manuscript has been published.

Competing interest: The authors declare that they have no competing interests.

Funding: US Department of Energy awards ER64408 and ER65286 to AOS

Authors' contributions: SL conceived and designed experiments, prepared biological samples, extracted ribosomal depleted RNA for RNA-Seq, performed all data analysis, and drafted manuscript. AOS was a major contributor in experimental design, feedback on data analysis, and in editing the manuscript. All authors read and approved the manuscript.

ACKNOWLEDGMENTS

We thank Roger Nilsen at the Georgia Genomics Facility for library preparation and Sharron Crane at Rutgers University for Hg content analysis. We also thank Bryndan Durham, Brandon Satinsky, Mary Ann Moran, Michael K. Johnson, Harry Dailey, Timothy Hoover, Anna Karls, Alexander Johs, Jerry Parks, Susan Miller, and Andrew Wiggins who have provided feedback and discussion on this work. This work was supported by US Department of Energy awards ER64408 and ER65286 to AOS.

REFERENCES

1. Driscoll CT, Mason RP, Chan HM, Jacob DJ, Pirrone N. Mercury as a global pollutant: sources, pathways, and effects. *Environ Sci Technol.* 2013;47(10):4967-4983.

bioRxiv preprint doi: https://doi.org/10.1101/161646; this version posted July 10, 2017. The copyright holder for this preprint (which was not certified by peer review) is the author/funder, who has granted bioRxiv a license to display the preprint in perpetuity. It is made available under aCC-BY-NC-ND 4.0 International license.

2. Pirrone N, Cinnirella S, Feng X, Finkelman RB, Friedli HR, Leaner J, Mason R, Mukherjee AB, Stracher G, Streets DG *et al*: Global Mercury Emissions to the Atmosphere from Natural and Anthropogenic Sources. In: Mason R, Pirrone N, editors. *Mercury Fate and Transport in the Global Atmosphere: Emissions, Measurements and Models.* Boston, MA: Springer US;2009. p. 1-47.

3. Mason RP, Fitzgerald WF, Morel FMM. The Biogeochemical Cycling of Elemental Mercury - Anthropogenic Influences. *Geochimica Et Cosmochimica Acta.* 1994;58:3191-3198.

4. Barkay T, Miller SM, Summers AO. Bacterial mercury resistance from atoms to ecosystems. *FEMS Microbiol Rev.* 2003;27(2-3):355-384.

5. Crinnion WJ. Environmental medicine, part three: long-term effects of chronic low-dose mercury exposure. *Alternative medicine review : a journal of clinical therapeutic.* 2000;5(3):209-223.

6. Richardson GM, Wilson R, Allard D, Purtill C, Douma S, Graviere J. Mercury exposure and risks from dental amalgam in the US population, post-2000. *The Science of the total environment.* 2011;409(20):4257-4268.

7. Diez S. Human health effects of methylmercury exposure. *Rev Environ Contam Toxicol.* 2009;198:111-132.

8. Malm O. Gold mining as a source of mercury exposure in the Brazilian Amazon. *Environ Res.* 1998;77(2):73-78.

bioRxiv preprint doi: https://doi.org/10.1101/161646; this version posted July 10, 2017. The copyright holder for this preprint (which was not certified by peer review) is the author/funder, who has granted bioRxiv a license to display the preprint in perpetuity. It is made available under aCC-BY-NC-ND 4.0 International license.

1091 9. Clarkson TW, Magos L. The toxicology of mercury and its chemical compounds.
1092 *Crit Rev Toxicol.* 2006;36(8):609-662.

1093 10. Hintelmann H, Hempel M, Wilken RD. Observation of unusual organic mercury
1094 species in soils and sediments of industrially contaminated sites. *Environ Sci Technol.*
1095 1995;29(7):1845-1850.

1096 11. Tchounwou PB, Ayensu WK, Ninashvili N, Sutton D. Environmental exposure to
1097 mercury and its toxicopathologic implications for public health. *Environ Toxicol.*
1098 2003;18(3):149-175.

1099 12. Davidson PW, Myers GJ, Weiss B. Mercury exposure and child development
1100 outcomes. *Pediatrics.* 2004;113(Suppl 4):1023-1029.

1101 13. Valko M, Morris H, Cronin MT. Metals, toxicity and oxidative stress. *Curr Med*
1102 *Chem.* 2005;12(10):1161-1208.

1103 14. Yorifuji T, Tsuda T, Takao S, Harada M. Long-term exposure to methylmercury
1104 and neurologic signs in Minamata and neighboring communities. *Epidemiology.*
1105 2008;19(1):3-9.

1106 15. Zahir F, Rizwi SJ, Haq SK, Khan RH. Low dose mercury toxicity and human
1107 health. *Environ Toxicol Pharmacol.* 2005;20(2):351-360.

1108 16. Cheesman BV, Arnold AP, Rabenstein DL. Nuclear magnetic resonance studies
1109 of the solution chemistry of metal complexes. 25. Hg(thiol)3 complexes and HG(II)-thiol
1110 ligand exchange kinetics. *J Am Chem Soc.* 1988;110:6359-6364.

bioRxiv preprint doi: https://doi.org/10.1101/161646; this version posted July 10, 2017. The copyright holder for this preprint (which was not certified by peer review) is the author/funder, who has granted bioRxiv a license to display the preprint in perpetuity. It is made available under aCC-BY-NC-ND 4.0 International license.

17. Oram PD, Fang X, Fernando Q, Letkeman P, Letkeman D. The formation of constants of mercury(II)--glutathione complexes. *Chemical research in toxicology.* 1996;9(4):709-712.

18. Labunskyy VM, Hatfield DL, Gladyshev VN. Selenoproteins: molecular pathways and physiological roles. *Physiol Rev.* 2014;94(3):739-777.

19. Pal PB, Pal S, Das J, Sil PC. Modulation of mercury-induced mitochondria-dependent apoptosis by glycine in hepatocytes. *Amino Acids.* 2012;42(5):1669-1683.

20. Shenker BJ, Guo TL, Shapiro IM. Mercury-induced apoptosis in human lymphoid cells: evidence that the apoptotic pathway is mercurial species dependent. *Environ Res.* 2000;84(2):89-99.

21. Jomova K, Valko M. Advances in metal-induced oxidative stress and human disease. *Toxicology.* 2011;283(2-3):65-87.

22. Polacco BJ, Purvine SO, Zink EM, Lavoie SP, Lipton MS, Summers AO, Miller SM. Discovering mercury protein modifications in whole proteomes using natural isotope distributions observed in liquid chromatography-tandem mass spectrometry. *Mol Cell Proteomics.* 2011;10(8):M110.004853.

23. LaVoie SP, Mapolelo DT, Cowart DM, Polacco BJ, Johnson MK, Scott RA, Miller SM, Summers AO. Organic and inorganic mercurials have distinct effects on cellular thiols, metal homeostasis, and Fe-binding proteins in Escherichia coli. *J Biol Inorg Chem.* 2015;20(8):1239-1251.

bioRxiv preprint doi: https://doi.org/10.1101/161646; this version posted July 10, 2017. The copyright holder for this preprint (which was not certified by peer review) is the author/funder, who has granted bioRxiv a license to display the preprint in perpetuity. It is made available under aCC-BY-NC-ND 4.0 International license.

1131 24. McElwee MK, Ho LA, Chou JW, Smith MV, Freedman JH. Comparative
1132 toxicogenomic responses of mercuric and methyl-mercury. *BMC Genomics.*
1133 2013;14:698.

1134 25. Neidhardt FC, Bloch PL, Smith DF. Culture medium for enterobacteria. *Journal of*
1135 *bacteriology.* 1974;119(3):736-747.

1136 26. Stead MB, Agrawal A, Bowden KE, Nasir R, Mohanty BK, Meagher RB, Kushner
1137 SR. RNAsnap: a rapid, quantitative and inexpensive, method for isolating total RNA
1138 from bacteria. *Nucleic acids research.* 2012;40(20):e156.

1139 27. Langmead B, Salzberg SL. Fast gapped-read alignment with Bowtie 2. *Nature*
1140 *methods.* 2012;9(4):357-359.

1141 28. Li H, Handsaker B, Wysoker A, Fennell T, Ruan J, Homer N, Marth G, Abecasis
1142 G, Durbin R, Genome Project Data Processing S. The Sequence Alignment/Map format
1143 and SAMtools. *Bioinformatics.* 2009;25(16):2078-2079.

1144 29. Anders S, Pyl PT, Huber W. HTSeq--a Python framework to work with high-
1145 throughput sequencing data. *Bioinformatics.* 2015;31(2):166-169.

1146 30. Hardcastle TJ, Kelly KA. baySeq: empirical Bayesian methods for identifying
1147 differential expression in sequence count data. *BMC bioinformatics.* 2010;11:422.

1148 31. Hamlett NV, Landale EC, Davis BH, Summers AO. Roles of the Tn21 merT,
1149 merP, and merC gene products in mercury resistance and mercury binding. *Journal of*
1150 *bacteriology.* 1992;174(20):6377-6385.

bioRxiv preprint doi: https://doi.org/10.1101/161646; this version posted July 10, 2017. The copyright holder for this preprint (which was not certified by peer review) is the author/funder, who has granted bioRxiv a license to display the preprint in perpetuity. It is made available under aCC-BY-NC-ND 4.0 International license.

1151 32. Summers AO, Lewis E. Volatilization of mercuric chloride by mercury-resistant
1152 plasmid-bearing strains of Escherichia coli, Staphylococcus aureus, and Pseudomonas
1153 aeruginosa. *Journal of bacteriology.* 1973;113(2):1070-1072.

1154 33. Summers AO, Silver S. Mercury resistance in a plasmid-bearing strain of
1155 Escherichia coli. *Journal of bacteriology.* 1972;112(3):1228-1236.

1156 34. Schaechter M, Santomassino KA. Lysis of Escherichia coli by sulfhydryl-binding
1157 reagents. *Journal of bacteriology.* 1962;84:318-325.

1158 35. Janssen BD, Hayes CS. The tmRNA ribosome-rescue system. *Adv Protein*
1159 *Chem Struct Biol.* 2012;86:151-191.

1160 36. Legendre P. Ward's Hierarchical Agglomerative Clustering Method: Which
1161 Algorithms Implement Ward's Criterion? *Journal of Classification.* 2014;31(3):274-295.

1162 37. Szklarczyk D, Franceschini A, Wyder S, Forslund K, Heller D, Huerta-Cepas J,
1163 Simonovic M, Roth A, Santos A, Tsafou KP *et al*. STRING v10: protein-protein
1164 interaction networks, integrated over the tree of life. *Nucleic acids research.*
1165 2015;43(Database issue):D447-452.

1166 38. von Mering C, Jensen LJ, Snel B, Hooper SD, Krupp M, Foglierini M, Jouffre N,
1167 Huynen MA, Bork P. STRING: known and predicted protein-protein associations,
1168 integrated and transferred across organisms. *Nucleic acids research.*
1169 2005;33(Database issue):D433-437.

bioRxiv preprint doi: https://doi.org/10.1101/161646; this version posted July 10, 2017. The copyright holder for this preprint (which was not certified by peer review) is the author/funder, who has granted bioRxiv a license to display the preprint in perpetuity. It is made available under aCC-BY-NC-ND 4.0 International license.

1170 39. Arunasri K, Adil M, Khan PA, Shivaji S. Global gene expression analysis of long-
1171 term stationary phase effects in E. coli K12 MG1655. *PLoS One.* 2014;9(5):e96701.

1172 40. Chang DE, Smalley DJ, Conway T. Gene expression profiling of Escherichia coli
1173 growth transitions: an expanded stringent response model. *Mol Microbiol.*
1174 2002;45(2):289-306.

1175 41. Kuzminov A. Recombinational repair of DNA damage in Escherichia coli and
1176 bacteriophage lambda. *Microbiol Mol Biol Rev.* 1999;63(4):751-813.

1177 42. Lusetti SL, Cox MM. The bacterial RecA protein and the recombinational DNA
1178 repair of stalled replication forks. *Annu Rev Biochem.* 2002;71:71-100.

1179 43. Salgado H, Martinez-Flores I, Lopez-Fuentes A, Garcia-Sotelo JS, Porron-Sotelo
1180 L, Solano H, Muniz-Rascado L, Collado-Vides J. Extracting regulatory networks of
1181 Escherichia coli from RegulonDB. *Methods Mol Biol.* 2012;804:179-195.

1182 44. Salgado H, Peralta-Gil M, Gama-Castro S, Santos-Zavaleta A, Muniz-Rascado L,
1183 Garcia-Sotelo JS, Weiss V, Solano-Lira H, Martinez-Flores I, Medina-Rivera A *et al*.
1184 RegulonDB v8.0: omics data sets, evolutionary conservation, regulatory phrases, cross-
1185 validated gold standards and more. *Nucleic acids research.* 2013;41(Database
1186 issue):D203-213.

1187 45. Tramonti A, Visca P, De Canio M, Falconi M, De Biase D. Functional
1188 characterization and regulation of gadX, a gene encoding an AraC/XylS-like
1189 transcriptional activator of the Escherichia coli glutamic acid decarboxylase system.
1190 *Journal of bacteriology.* 2002;184(10):2603-2613.

bioRxiv preprint doi: https://doi.org/10.1101/161646; this version posted July 10, 2017. The copyright holder for this preprint (which was not certified by peer review) is the author/funder, who has granted bioRxiv a license to display the preprint in perpetuity. It is made available under aCC-BY-NC-ND 4.0 International license.

1191 46. Nishino K, Senda Y, Yamaguchi A. The AraC-family regulator GadX enhances
1192 multidrug resistance in Escherichia coli by activating expression of mdtEF multidrug
1193 efflux genes. *J Infect Chemother.* 2008;14(1):23-29.

1194 47. Tucker DL, Tucker N, Ma Z, Foster JW, Miranda RL, Cohen PS, Conway T.
1195 Genes of the GadX-GadW regulon in Escherichia coli. *Journal of bacteriology.*
1196 2003;185(10):3190-3201.

1197 48. Lemke JJ, Sanchez-Vazquez P, Burgos HL, Hedberg G, Ross W, Gourse RL.
1198 Direct regulation of Escherichia coli ribosomal protein promoters by the transcription
1199 factors ppGpp and DksA. *Proc Natl Acad Sci U S A.* 2011;108(14):5712-5717.

1200 49. Nomura M, Gourse R, Baughman G. Regulation of the synthesis of ribosomes
1201 and ribosomal components. *Annu Rev Biochem.* 1984;53:75-117.

1202 50. Wilson DN, Nierhaus KH. The weird and wonderful world of bacterial ribosome
1203 regulation. *Crit Rev Biochem Mol Biol.* 2007;42(3):187-219.

1204 51. Soskine M, Steiner-Mordoch S, Schuldiner S. Crosslinking of membrane-
1205 embedded cysteines reveals contact points in the EmrE oligomer. *Proc Natl Acad Sci U*
1206 *S A.* 2002;99(19):12043-12048.

1207 52. Imesch E, Moosmayer M, Anner BM. Mercury weakens membrane anchoring of
1208 Na-K-ATPase. *The American journal of physiology.* 1992;262(5):F837-842.

bioRxiv preprint doi: https://doi.org/10.1101/161646; this version posted July 10, 2017. The copyright holder for this preprint (which was not certified by peer review) is the author/funder, who has granted bioRxiv a license to display the preprint in perpetuity. It is made available under aCC-BY-NC-ND 4.0 International license.

1209 53. Carvalho CM, Chew EH, Hashemy SI, Lu J, Holmgren A. Inhibition of the human
1210 thioredoxin system. A molecular mechanism of mercury toxicity. *J Biol Chem.*
1211 2008;283(18):11913-11923.

1212 54. Georgopoulos C, Welch WJ. Role of the major heat shock proteins as molecular
1213 chaperones. *Annu Rev Cell Biol.* 1993;9:601-634.

1214 55. Carpousis AJ. The RNA degradosome of Escherichia coli: an mRNA-degrading
1215 machine assembled on RNase E. *Annu Rev Microbiol.* 2007;61:71-87.

1216 56. Lim JY, May JM, Cegelski L. Dimethyl sulfoxide and ethanol elicit increased
1217 amyloid biogenesis and amyloid-integrated biofilm formation in Escherichia coli. *Appl*
1218 *Environ Microbiol.* 2012;78(9):3369-3378.

1219 57. Markarian SA, Poladyan AA, Kirakosyan GR, Trchounian AA, Bagramyan KA.
1220 Effect of diethylsulphoxide on growth, survival and ion exchange of Escherichia coli. *Lett*
1221 *Appl Microbiol.* 2002;34(6):417-421.

1222 58. Ansaldi M, Bordi C, Lepelletier M, Mejean V. TorC apocytochrome negatively
1223 autoregulates the trimethylamine N-oxide (TMAO) reductase operon in Escherichia coli.
1224 *Mol Microbiol.* 1999;33(2):284-295.

1225 59. Sorensen KI, Hove-Jensen B. Ribose catabolism of Escherichia coli:
1226 characterization of the rpiB gene encoding ribose phosphate isomerase B and of the
1227 rpiR gene, which is involved in regulation of rpiB expression. *Journal of bacteriology.*
1228 1996;178(4):1003-1011.

bioRxiv preprint doi: https://doi.org/10.1101/161646; this version posted July 10, 2017. The copyright holder for this preprint (which was not certified by peer review) is the author/funder, who has granted bioRxiv a license to display the preprint in perpetuity. It is made available under aCC-BY-NC-ND 4.0 International license.

1229 60. Yamada T, Letunic I, Okuda S, Kanehisa M, Bork P. iPath2.0: interactive
1230 pathway explorer. *Nucleic acids research.* 2011;39(Web Server issue):W412-415.

1231 61. Imlay JA. The molecular mechanisms and physiological consequences of
1232 oxidative stress: lessons from a model bacterium. *Nat Rev Microbiol.* 2013;11(7):443-
1233 454.

1234 62. Grass G, Otto M, Fricke B, Haney CJ, Rensing C, Nies DH, Munkelt D. FieF
1235 (YiiP) from Escherichia coli mediates decreased cellular accumulation of iron and
1236 relieves iron stress. *Arch Microbiol.* 2005;183(1):9-18.

1237 63. Bandyopadhyay S, Chandramouli K, Johnson MK. Iron-sulfur cluster
1238 biosynthesis. *Biochem Soc Trans.* 2008;36(Pt 6):1112-1119.

1239 64. Johnson DC, Dean DR, Smith AD, Johnson MK. Structure, function, and
1240 formation of biological iron-sulfur clusters. *Annu Rev Biochem.* 2005;74:247-281.

1241 65. Rensing C, Mitra B, Rosen BP. The zntA gene of Escherichia coli encodes a
1242 Zn(II)-translocating P-type ATPase. *Proc Natl Acad Sci U S A.* 1997;94(26):14326-
1243 14331.

1244 66. Outten FW, Huffman DL, Hale JA, O'Halloran TV. The independent cue and cus
1245 systems confer copper tolerance during aerobic and anaerobic growth in Escherichia
1246 coli. *J Biol Chem.* 2001;276(33):30670-30677.

1247 67. Eitinger T, Mandrand-Berthelot MA. Nickel transport systems in microorganisms.
1248 *Arch Microbiol.* 2000;173(1):1-9.

bioRxiv preprint doi: https://doi.org/10.1101/161646; this version posted July 10, 2017. The copyright holder for this preprint (which was not certified by peer review) is the author/funder, who has granted bioRxiv a license to display the preprint in perpetuity. It is made available under aCC-BY-NC-ND 4.0 International license.

1249 68. Qin J, Fu HL, Ye J, Bencze KZ, Stemmler TL, Rawlings DE, Rosen BP.
1250 Convergent evolution of a new arsenic binding site in the ArsR/SmtB family of
1251 metalloregulators. *J Biol Chem.* 2007;282(47):34346-34355.

1252 69. Alekshun MN, Levy SB. The mar regulon: multiple resistance to antibiotics and
1253 other toxic chemicals. *Trends Microbiol.* 1999;7(10):410-413.

1254 70. Nishino K, Yamada J, Hirakawa H, Hirata T, Yamaguchi A. Roles of TolC-
1255 dependent multidrug transporters of Escherichia coli in resistance to beta-lactams.
1256 *Antimicrob Agents Chemother.* 2003;47(9):3030-3033.

1257 71. Raetz CR, Reynolds CM, Trent MS, Bishop RE. Lipid A modification systems in
1258 gram-negative bacteria. *Annu Rev Biochem.* 2007;76:295-329.

1259 72. Checroun C, Gutierrez C. Sigma(s)-dependent regulation of yehZYXW, which
1260 encodes a putative osmoprotectant ABC transporter of Escherichia coli. *FEMS Microbiol*
1261 *Lett.* 2004;236(2):221-226.

1262 73. Van Houdt R, Michiels CW. Role of bacterial cell surface structures in
1263 Escherichia coli biofilm formation. *Res Microbiol.* 2005;156(5-6):626-633.

1264 74. Ma Q, Zhang G, Wood TK. Escherichia coli BdcA controls biofilm dispersal in
1265 Pseudomonas aeruginosa and Rhizobium meliloti. *BMC Res Notes.* 2011;4:447.

1266 75. Zhang XS, Garcia-Contreras R, Wood TK. YcfR (BhsA) influences Escherichia
1267 coli biofilm formation through stress response and surface hydrophobicity. *Journal of*
1268 *bacteriology.* 2007;189(8):3051-3062.

bioRxiv preprint doi: https://doi.org/10.1101/161646; this version posted July 10, 2017. The copyright holder for this preprint (which was not certified by peer review) is the author/funder, who has granted bioRxiv a license to display the preprint in perpetuity. It is made available under aCC-BY-NC-ND 4.0 International license.

1269 76. Itoh Y, Rice JD, Goller C, Pannuri A, Taylor J, Meisner J, Beveridge TJ, Preston
1270 JF, 3rd, Romeo T. Roles of pgaABCD genes in synthesis, modification, and export of
1271 the Escherichia coli biofilm adhesin poly-beta-1,6-N-acetyl-D-glucosamine. *Journal of*
1272 *bacteriology.* 2008;190(10):3670-3680.

1273 77. Lee J, Page R, Garcia-Contreras R, Palermino JM, Zhang XS, Doshi O, Wood
1274 TK, Peti W. Structure and function of the Escherichia coli protein YmgB: a protein
1275 critical for biofilm formation and acid-resistance. *J Mol Biol.* 2007;373(1):11-26.

1276 78. Cegelski L, Pinkner JS, Hammer ND, Cusumano CK, Hung CS, Chorell E, Aberg
1277 V, Walker JN, Seed PC, Almqvist F *et al*. Small-molecule inhibitors target Escherichia
1278 coli amyloid biogenesis and biofilm formation. *Nat Chem Biol.* 2009;5(12):913-919.

1279 79. Seo SW, Kim D, Szubin R, Palsson BO. Genome-wide Reconstruction of OxyR
1280 and SoxRS Transcriptional Regulatory Networks under Oxidative Stress in Escherichia
1281 coli K-12 MG1655. *Cell Rep.* 2015;12(8):1289-1299.

1282 80. Choi H, Kim S, Mukhopadhyay P, Cho S, Woo J, Storz G, Ryu SE. Structural
1283 basis of the redox switch in the OxyR transcription factor. *Cell.* 2001;105(1):103-113.

1284 81. Altuvia S, Zhang A, Argaman L, Tiwari A, Storz G. The Escherichia coli OxyS
1285 regulatory RNA represses fhlA translation by blocking ribosome binding. *EMBO J.*
1286 1998;17(20):6069-6075.

1287 82. Amabile-Cuevas CF, Demple B. Molecular characterization of the soxRS genes
1288 of Escherichia coli: two genes control a superoxide stress regulon. *Nucleic acids*
1289 *research.* 1991;19(16):4479-4484.

bioRxiv preprint doi: https://doi.org/10.1101/161646; this version posted July 10, 2017. The copyright holder for this preprint (which was not certified by peer review) is the author/funder, who has granted bioRxiv a license to display the preprint in perpetuity. It is made available under aCC-BY-NC-ND 4.0 International license.

1290 83. Greenberg JT, Monach P, Chou JH, Josephy PD, Demple B. Positive control of a
1291 global antioxidant defense regulon activated by superoxide-generating agents in
1292 Escherichia coli. *Proc Natl Acad Sci U S A.* 1990;87(16):6181-6185.

1293 84. Tsaneva IR, Weiss B. soxR, a locus governing a superoxide response regulon in
1294 Escherichia coli K-12. *Journal of bacteriology.* 1990;172(8):4197-4205.

1295 85. Watanabe S, Kita A, Kobayashi K, Miki K. Crystal structure of the [2Fe-2S]
1296 oxidative-stress sensor SoxR bound to DNA. *Proc Natl Acad Sci U S A.*
1297 2008;105(11):4121-4126.

1298 86. Keseler IM, Mackie A, Peralta-Gil M, Santos-Zavaleta A, Gama-Castro S,
1299 Bonavides-Martinez C, Fulcher C, Huerta AM, Kothari A, Krummenacker M *et al*.
1300 EcoCyc: fusing model organism databases with systems biology. *Nucleic acids*
1301 *research.* 2013;41(Database issue):D605-612.

1302 87. Anjem A, Varghese S, Imlay JA. Manganese import is a key element of the OxyR
1303 response to hydrogen peroxide in Escherichia coli. *Mol Microbiol.* 2009;72(4):844-858.

1304 88. Park SJ, Gunsalus RP. Oxygen, iron, carbon, and superoxide control of the
1305 fumarase fumA and fumC genes of Escherichia coli: role of the arcA, fnr, and soxR
1306 gene products. *Journal of bacteriology.* 1995;177(21):6255-6262.

1307 89. Varghese S, Tang Y, Imlay JA. Contrasting sensitivities of Escherichia coli
1308 aconitases A and B to oxidation and iron depletion. *Journal of bacteriology.*
1309 2003;185(1):221-230.

bioRxiv preprint doi: https://doi.org/10.1101/161646; this version posted July 10, 2017. The copyright holder for this preprint (which was not certified by peer review) is the author/funder, who has granted bioRxiv a license to display the preprint in perpetuity. It is made available under aCC-BY-NC-ND 4.0 International license.

1310 90. Eser M, Masip L, Kadokura H, Georgiou G, Beckwith J. Disulfide bond formation
1311 by exported glutaredoxin indicates glutathione's presence in the E. coli periplasm. *Proc*
1312 *Natl Acad Sci U S A.* 2009;106(5):1572-1577.

1313 91. Suzuki H, Koyanagi T, Izuka S, Onishi A, Kumagai H. The yliA, -B, -C, and -D
1314 genes of Escherichia coli K-12 encode a novel glutathione importer with an ATP-binding
1315 cassette. *Journal of bacteriology.* 2005;187(17):5861-5867.

1316 92. Vuilleumier S. Bacterial glutathione S-transferases: what are they good for?
1317 *Journal of bacteriology.* 1997;179(5):1431-1441.

1318 93. Summers AO, Wireman J, Vimy MJ, Lorscheider FL, Marshall B, Levy SB,
1319 Bennett S, Billard L. Mercury released from dental "silver" fillings provokes an increase
1320 in mercury- and antibiotic-resistant bacteria in oral and intestinal floras of primates.
1321 *Antimicrob Agents Chemother.* 1993;37(4):825-834.

1322 94. US - Food & Drug Administration (FDA): Mercury Levels in Commercial Fish and
1323 Shellfish (1990-2012)
1324 http://www.fda.gov/Food/FoodborneIllnessContaminants/Metals/ucm115644.htm

1325 95. McElwee MK, Freedman JH. Comparative toxicology of mercurials in
1326 Caenorhabditis elegans. *Environ Toxicol Chem.* 2011;30(9):2135-2141.

1327 96. Ung CY, Lam SH, Hlaing MM, Winata CL, Korzh S, Mathavan S, Gong Z.
1328 Mercury-induced hepatotoxicity in zebrafish: in vivo mechanistic insights from
1329 transcriptome analysis, phenotype anchoring and targeted gene expression validation.
1330 *BMC Genomics.* 2010;11:212.

bioRxiv preprint doi: https://doi.org/10.1101/161646; this version posted July 10, 2017. The copyright holder for this preprint (which was not certified by peer review) is the author/funder, who has granted bioRxiv a license to display the preprint in perpetuity. It is made available under aCC-BY-NC-ND 4.0 International license.

1331 97. Lash LH, Zalups RK. Alterations in renal cellular glutathione metabolism after in
1332 vivo administration of a subtoxic dose of mercuric chloride. *J Biochem Toxicol.*
1333 1996;11(1):1-9.

1334 98. Lu X, Xiang Y, Yang G, Zhang L, Wang H, Zhong S. Transcriptomic
1335 characterization of zebrafish larvae in response to mercury exposure. *Comp Biochem*
1336 *Physiol C Toxicol Pharmacol.* 2017;192:40-49.

1337 99. Zheng M, Wang X, Templeton LJ, Smulski DR, LaRossa RA, Storz G. DNA
1338 microarray-mediated transcriptional profiling of the Escherichia coli response to
1339 hydrogen peroxide. *Journal of bacteriology.* 2001;183(15):4562-4570.

1340 100. Kanai T, Takahashi K, Inoue H. Three distinct-type glutathione S-transferases
1341 from Escherichia coli important for defense against oxidative stress. *J Biochem.*
1342 2006;140(5):703-711.

1343 101. Xu FF, Imlay JA. Silver(I), mercury(II), cadmium(II), and zinc(II) target exposed
1344 enzymic iron-sulfur clusters when they toxify Escherichia coli. *Appl Environ Microbiol.*
1345 2012;78(10):3614-3621.

1346 102. Varghese S, Wu A, Park S, Imlay KR, Imlay JA. Submicromolar hydrogen
1347 peroxide disrupts the ability of Fur protein to control free-iron levels in Escherichia coli.
1348 *Mol Microbiol.* 2007;64(3):822-830.

1349 103. Bagg A, Neilands JB. Ferric uptake regulation protein acts as a repressor,
1350 employing iron (II) as a cofactor to bind the operator of an iron transport operon in
1351 Escherichia coli. *Biochemistry.* 1987;26(17):5471-5477.

bioRxiv preprint doi: https://doi.org/10.1101/161646; this version posted July 10, 2017. The copyright holder for this preprint (which was not certified by peer review) is the author/funder, who has granted bioRxiv a license to display the preprint in perpetuity. It is made available under aCC-BY-NC-ND 4.0 International license.

1352 104. de Lorenzo V, Wee S, Herrero M, Neilands JB. Operator sequences of the
1353 aerobactin operon of plasmid ColV-K30 binding the ferric uptake regulation (fur)
1354 repressor. *Journal of bacteriology.* 1987;169(6):2624-2630.

1355 105. Fontecave M, Choudens SO, Py B, Barras F. Mechanisms of iron-sulfur cluster
1356 assembly: the SUF machinery. *J Biol Inorg Chem.* 2005;10(7):713-721.

1357 106. Zhao G, Ceci P, Ilari A, Giangiacomo L, Laue TM, Chiancone E, Chasteen ND.
1358 Iron and hydrogen peroxide detoxification properties of DNA-binding protein from
1359 starved cells. A ferritin-like DNA-binding protein of Escherichia coli. *J Biol Chem.*
1360 2002;277(31):27689-27696.

1361 107. Lund BO, Miller DM, Woods JS. Mercury-induced H2O2 production and lipid
1362 peroxidation in vitro in rat kidney mitochondria. *Biochem Pharmacol.* 1991;42
1363 Suppl:S181-187.

1364 108. Liochev SI, Fridovich I. Modulation of the fumarases of Escherichia coli in
1365 response to oxidative stress. *Arch Biochem Biophys.* 1993;301(2):379-384.

1366 109. Martin JE, Imlay JA. The alternative aerobic ribonucleotide reductase of
1367 Escherichia coli, NrdEF, is a manganese-dependent enzyme that enables cell
1368 replication during periods of iron starvation. *Mol Microbiol.* 2011;80(2):319-334.

1369 110. Jordan A, Aslund F, Pontis E, Reichard P, Holmgren A. Characterization of
1370 Escherichia coli NrdH. A glutaredoxin-like protein with a thioredoxin-like activity profile. *J*
1371 *Biol Chem.* 1997;272(29):18044-18050.

bioRxiv preprint doi: https://doi.org/10.1101/161646; this version posted July 10, 2017. The copyright holder for this preprint (which was not certified by peer review) is the author/funder, who has granted bioRxiv a license to display the preprint in perpetuity. It is made available under aCC-BY-NC-ND 4.0 International license.

1372 111. Sharma SK, Goloubinoff P, Christen P. Heavy metal ions are potent inhibitors of
1373 protein folding. *Biochem Biophys Res Commun.* 2008;372(2):341-345.

1374 112. Arsene F, Tomoyasu T, Bukau B. The heat shock response of Escherichia coli.
1375 *Int J Food Microbiol.* 2000;55(1-3):3-9.

1376 113. Bissonnette SA, Rivera-Rivera I, Sauer RT, Baker TA. The IbpA and IbpB small
1377 heat-shock proteins are substrates of the AAA+ Lon protease. *Mol Microbiol.*
1378 2010;75(6):1539-1549.

1379 114. Gaubig LC, Waldminghaus T, Narberhaus F. Multiple layers of control govern
1380 expression of the Escherichia coli ibpAB heat-shock operon. *Microbiology.* 2011;157(Pt
1381 1):66-76.

1382 115. Matuszewska E, Kwiatkowska J, Kuczynska-Wisnik D, Laskowska E. Escherichia
1383 coli heat-shock proteins IbpA/B are involved in resistance to oxidative stress induced by
1384 copper. *Microbiology.* 2008;154(Pt 6):1739-1747.

1385 116. Wang A, Crowley DE. Global gene expression responses to cadmium toxicity in
1386 Escherichia coli. *Journal of bacteriology.* 2005;187(9):3259-3266.

1387 117. Salmon K, Hung SP, Mekjian K, Baldi P, Hatfield GW, Gunsalus RP. Global gene
1388 expression profiling in Escherichia coli K12. The effects of oxygen availability and FNR.
1389 *J Biol Chem.* 2003;278(32):29837-29855.

1390 118. Bibikov SI, Biran R, Rudd KE, Parkinson JS. A signal transducer for aerotaxis in
1391 Escherichia coli. *Journal of bacteriology.* 1997;179(12):4075-4079.

bioRxiv preprint doi: https://doi.org/10.1101/161646; this version posted July 10, 2017. The copyright holder for this preprint (which was not certified by peer review) is the author/funder, who has granted bioRxiv a license to display the preprint in perpetuity. It is made available under aCC-BY-NC-ND 4.0 International license.

1392 119. Pruss BM, Campbell JW, Van Dyk TK, Zhu C, Kogan Y, Matsumura P. FlhD/FlhC
1393 is a regulator of anaerobic respiration and the Entner-Doudoroff pathway through
1394 induction of the methyl-accepting chemotaxis protein Aer. *Journal of bacteriology.*
1395 2003;185(2):534-543.

1396 120. Funk AE, Day FA, Brady FO. Displacement of zinc and copper from copper-
1397 induced metallothionein by cadmium and by mercury: in vivo and ex vivo studies. *Comp*
1398 *Biochem Physiol C.* 1987;86(1):1-6.

1399 121. O'Connor TR, Graves RJ, de Murcia G, Castaing B, Laval J. Fpg protein of
1400 Escherichia coli is a zinc finger protein whose cysteine residues have a structural and/or
1401 functional role. *J Biol Chem.* 1993;268(12):9063-9070.

1402 122. Binet MR, Poole RK. Cd(II), Pb(II) and Zn(II) ions regulate expression of the
1403 metal-transporting P-type ATPase ZntA in Escherichia coli. *FEBS Lett.* 2000;473(1):67-
1404 70.

1405 123. Sharma R, Rensing C, Rosen BP, Mitra B. The ATP hydrolytic activity of purified
1406 ZntA, a Pb(II)/Cd(II)/Zn(II)-translocating ATPase from Escherichia coli. *J Biol Chem.*
1407 2000;275(6):3873-3878.

1408 124. Fitzgerald DM, Bonocora RP, Wade JT. Comprehensive mapping of the
1409 Escherichia coli flagellar regulatory network. *PLoS Genet.* 2014;10(10):e1004649.

1410 125. Dong T, Yu R, Schellhorn H. Antagonistic regulation of motility and transcriptome
1411 expression by RpoN and RpoS in Escherichia coli. *Mol Microbiol.* 2011;79(2):375-386.

bioRxiv preprint doi: https://doi.org/10.1101/161646; this version posted July 10, 2017. The copyright holder for this preprint (which was not certified by peer review) is the author/funder, who has granted bioRxiv a license to display the preprint in perpetuity. It is made available under aCC-BY-NC-ND 4.0 International license.

126. De Lay N, Gottesman S. A complex network of small non-coding RNAs regulate motility in Escherichia coli. *Mol Microbiol.* 2012;86(3):524-538.

127. Mermod M, Magnani D, Solioz M, Stoyanov JV. The copper-inducible ComR (YcfQ) repressor regulates expression of ComC (YcfR), which affects copper permeability of the outer membrane of Escherichia coli. *Biometals.* 2012;25(1):33-43.

128. Schwechheimer C, Kuehn MJ. Outer-membrane vesicles from Gram-negative bacteria: biogenesis and functions. *Nat Rev Microbiol.* 2015;13(10):605-619.

129. Crepin S, Chekabab SM, Le Bihan G, Bertrand N, Dozois CM, Harel J. The Pho regulon and the pathogenesis of Escherichia coli. *Vet Microbiol.* 2011;153(1-2):82-88.

130. Hsieh YJ, Wanner BL. Global regulation by the seven-component Pi signaling system. *Curr Opin Microbiol.* 2010;13(2):198-203.

131. Hondorp ER, Matthews RG. Oxidative stress inactivates cobalamin-independent methionine synthase (MetE) in Escherichia coli. *PLoS Biol.* 2004;2(11):e336.

132. Brooks P, Davidson N. Mercury(II) Complexes of Imidazole and Histidine. *Journal of the American Chemical Society.* 1960;82(9):2118-2123.

133. Pal C, Bengtsson-Palme J, Kristiansson E, Larsson DG. Co-occurrence of resistance genes to antibiotics, biocides and metals reveals novel insights into their co-selection potential. *BMC Genomics.* 2015;16(1):964.

bioRxiv preprint doi: https://doi.org/10.1101/161646; this version posted July 10, 2017. The copyright holder for this preprint (which was not certified by peer review) is the author/funder, who has granted bioRxiv a license to display the preprint in perpetuity. It is made available under aCC-BY-NC-ND 4.0 International license.

134. Wireman J, Liebert CA, Smith T, Summers AO. Association of mercury resistance with antibiotic resistance in the gram-negative fecal bacteria of primates. *Appl Environ Microbiol.* 1997;63(11):4494-4503.

135. Mehta P, Casjens S, Krishnaswamy S. Analysis of the lambdoid prophage element e14 in the E. coli K-12 genome. *BMC Microbiol.* 2004;4:4.

136. Wang X, Kim Y, Ma Q, Hong SH, Pokusaeva K, Sturino JM, Wood TK. Cryptic prophages help bacteria cope with adverse environments. *Nat Commun.* 2010;1:147.

Table 1: Genes with ≥ 20 fold-change for at least two time points after $HgCl_2$ exposure (n = 25).

Gene ID	Gene Name	Product Description	Hg t10	Hg t30	Hg t60	PMA t10	PMA t30	PMA t60
b1112	**bhsA**	Biofilm, cell surface and signaling defects, YhcN family	**1949**	**563**	**94**	**46**	**21**	n.s.
b4458	oxyS	OxyS sRNA activates genes that detoxify oxidative damage	**1524**	**1292**	**150**	10	6	n.s.
b4249	bdcA	c-di-GMP-binding biofilm dispersal mediator protein	**596**	**79**	7	16	2	n.s.
b3686	**ibpB**	Chaperone, heat-inducible protein of HSP20 family	**402**	**124**	**281**	**37**	**211**	9
b0812	dps	Stress-induced Fe-binding and storage protein	**339**	**52**	n.s.	4	2	n.s.
b4248	yjgH	Putative reactive intermediate deaminase, UPF0076 family	**296**	**24**	3	6	2	n.s.
b0849	grxA	Glutaredoxin 1	**246**	**33**	n.s.	14	4	n.s.
b1144	ymfJ	Function unknown, e14 prophage	**185**	**39**	n.s.	3	3	n.s.
b2582	**trxC**	Thioredoxin 2, zinc-binding; Trx2	**134**	**50**	7	**24**	**24**	n.s.
b1147	ymfL	Function unknown, e14 prophage	**95**	**29**	n.s.	n.s.	3	n.s.
b1146	croE	Cro-like repressor, e14 prophage	**90**	**40**	n.s.	n.s.	n.s.	n.s.
b3687	**ibpA**	Chaperone, heat-inducible protein of HSP20 family	**86**	19	**41**	10	**28**	4
b2531	iscR	Transcriptional repressor for isc operon; contains Fe-S cluster	**62**	**48**	9	12	18	n.s.
b1148	ymfM	Function unknown, e14 prophage	**49**	**21**	n.s.	n.s.	n.s.	n.s.
b4599	yneM	function unknown, membrane-associated; regulated by PhoPQ	**38**	**36**	n.s.	3	3	n.s.
b2673	nrdH	NrdH-redoxin reducing oxidized NrdEF	**35**	**127**	**21**	7	14	n.s.
b4030	**psiE**	Pho regulon, regulated by phoB and cAMP	**35**	**64**	17	**38**	**59**	n.s.
b1684	sufA	Scaffold protein for assembly of iron-sulfur clusters	**32**	**39**	5	n.s.	3	n.s.
b1748	**astC**	Succinylornithine transaminase; carbon starvation protein	**30**	**31**	**25**	**34**	**36**	n.s.
b4663	**azuC**	Function unknown; membrane-associated	**27**	**25**	**36**	**41**	**49**	n.s.
b0484	copA	Copper-, silver-translocating P-type ATPase efflux pump	**25**	**20**	n.s.	5	n.s.	-10
b2674	nrdI	Flavodoxin required for NrdEF cluster assembly	**21**	**73**	**22**	4	7	n.s.
b1747	astA	Arginine succinyltransferase, arginine catabolism	10	**20**	**29**	9	14	n.s.
b1020	**phoH**	ATP-binding protein, function unknown	8	**71**	**221**	**61**	**365**	n.s.
b4002	zraP	Zn-dependent periplasmic chaperone	3	**27**	**43**	n.s.	n.s.	-3

Table is sorted by Hg at 10 min column. n.s. = not significantly different from unexposed culture and boldface highlights actual values ≥ 20-fold. Gene names in boldface have a ≥ 20 differential expression response to both Hg and PMA in at least one time point (n = 8).

Table 2: Genes with ≥ 20 fold-change in at least two time points for PMA exposure (n= 17).

Gene ID	Gene Name	Product Description	Hg t10	Hg t30	Hg t60	PMA t10	PMA t30	PMA t60
b3728	pstS	ABC phosphate transport system; periplasmic binding protein	n.s.	16	8	**86**	**165**	n.s.
b1020	**phoH**	ATP-binding protein, function unknown	8	**71**	**221**	**61**	**365**	n.s.
b0996	torC	c-Type cytochrome	n.s.	n.s.	n.s.	**55**	**65**	**77**
b4060	**yjcB**	Function unknown	**33**	11	12	**52**	**35**	n.s.
b0399	**phoB**	Positive response regulator for pho regulon	4	**22**	3	**51**	**105**	n.s.
b1530	**marR**	Transcription repressor of multiple antibiotic resistance	**26**	7	n.s.	**48**	**29**	n.s.
b1531	marA	Transcriptional activator for multiple antibiotic resistance;	15	9	n.s.	**46**	**31**	n.s.
b1112	**bhsA**	Biofilm, cell surface and signaling defects, YhcN family	**1949**	**563**	**94**	**46**	**21**	n.s.
b1532	marB	marRAB multiple antibiotic resistance operon	16	8	n.s.	**45**	**27**	n.s.
b4663	**azuC**	Function unknown; membrane-associated	**27**	**25**	**36**	**41**	**49**	n.s.
b4030	**psiE**	Pho regulon, regulated by phoB and cAMP	**35**	**64**	17	**38**	**59**	n.s.
b3686	**ibpB**	Chaperone, heat-inducible protein of HSP20 family	**402**	**124**	**281**	**37**	**211**	9
b1748	**astC**	Succinylornithine transaminase; carbon starvation protein	**30**	**31**	**25**	**34**	**36**	n.s.
b3469	**zntA**	Zn(II), Cd(II), and Pb(II) translocating P-type ATPase	**40**	19	8	**29**	**22**	n.s.
b2582	**trxC**	Thioredoxin 2, zinc-binding; Trx2	**134**	**50**	7	**24**	**24**	n.s.
b4354	yjiY	Predicted transporter, function unknown	n.s.	n.s.	n.s.	**20**	**77**	n.s.
b1625	cnu	OriC-binding complex H-NS/Cnu	n.s.	10	n.s.	**20**	**24**	n.s.

Table is sorted by PMA at 10 min column. n.s. = not significantly different from unexposed culture and boldface highlights actual values ≥ 20-fold. Gene names in boldface have a ≥ 20 differential expression response to both Hg and PMA in at least one time point (n = 11).

bioRxiv preprint doi: https://doi.org/10.1101/161646; this version posted July 10, 2017. The copyright holder for this preprint (which was not certified by peer review) is the author/funder, who has granted bioRxiv a license to display the preprint in perpetuity. It is made available under aCC-BY-NC-ND 4.0 International license.

Table 3: Changes in transcription factor gene expression. The sum of transcription factor genes either up-regulated or down-regulated is shown with the percentage of the total transcription factor genes in parenthesis; percent's do not total 100 because genes with no change compared to unexposed cells are not tabulated here. See details in Table S12.

Transcription Factors (n = 203)						
	Hg_t10	**Hg_t30**	**Hg_t60**	**PMA_t10**	**PMA_t30**	**PMA_t60**
up	63 (31)	46 (23)	14 (7)	86 (42)	78 (38)	1 (0.5)
down	28 (14)	28 (14)	13 (6)	22 (11)	23 (11)	2 (1)

bioRxiv preprint doi: https://doi.org/10.1101/161646; this version posted July 10, 2017. The copyright holder for this preprint (which was not certified by peer review) is the author/funder, who has granted bioRxiv a license to display the preprint in perpetuity. It is made available under aCC-BY-NC-ND 4.0 International license.

Figures:

a

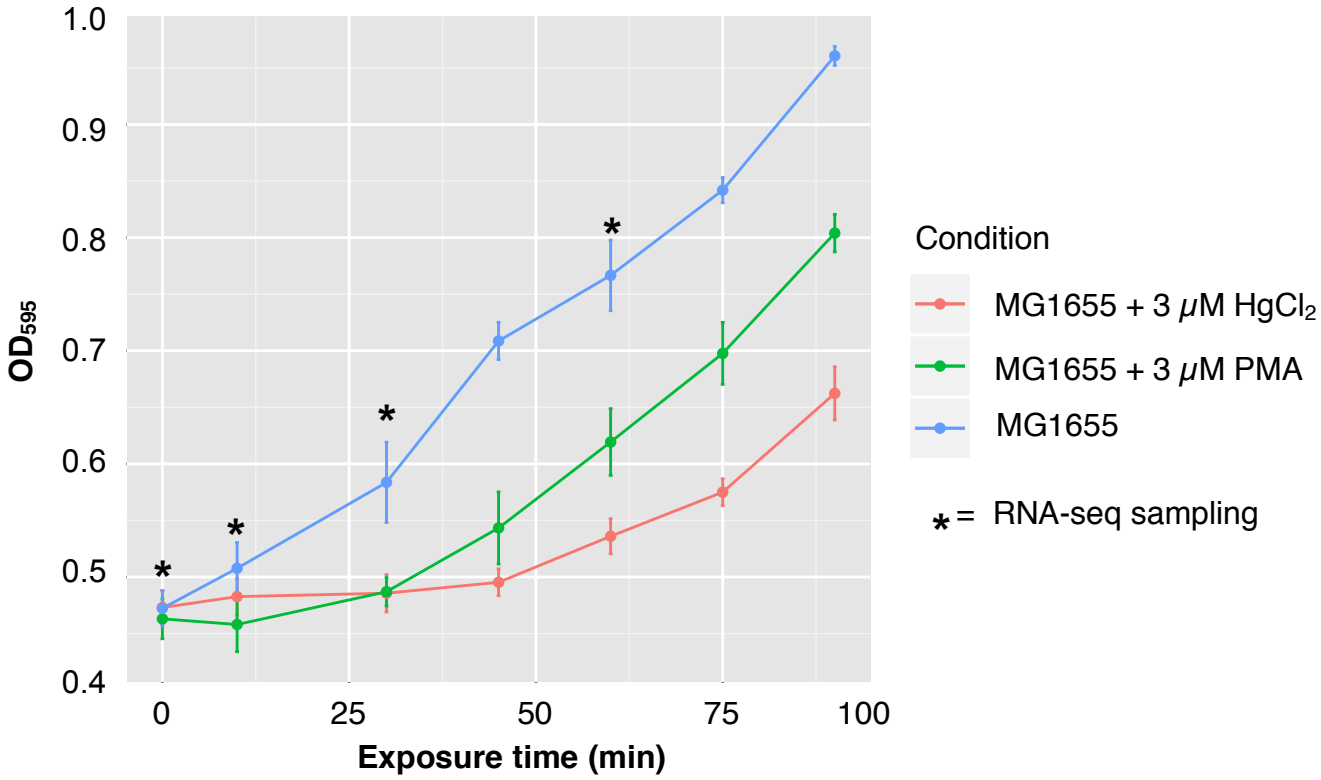

b

	t10	t30	t60
3μM $HgCl_2$	1,821 (894↑927↓)	1,422 (637↑785↓)	563 (259↑304↓)
3μM PMA	2,181 (1,261↑920↓)	2,009 (1,156↑853↓)	65 (36↑29↓)

Figure 1: Effects of sub-acute mercury exposure on growth of MG1655. (a) *E. coli* K12 MG1655 grown in MOPS minimal medium, unexposed (blue) or exposed to 3 μM $HgCl_2$ (red) or 3 μM PMA (green) during mid-log phase. Asterisks indicate sampling times for RNA-seq. Error bars are standard error (SEM) of 3 biological replicates for each culture condition. See Figure S1 for full growth curve. **(b)** Differentially expressed genes (DEG) counts (up or down) for $HgCl_2$ and PMA relative to unexposed control culture at each time point.

bioRxiv preprint doi: https://doi.org/10.1101/161646; this version posted July 10, 2017. The copyright holder for this preprint (which was not certified by peer review) is the author/funder, who has granted bioRxiv a license to display the preprint in perpetuity. It is made available under aCC-BY-NC-ND 4.0 International license.

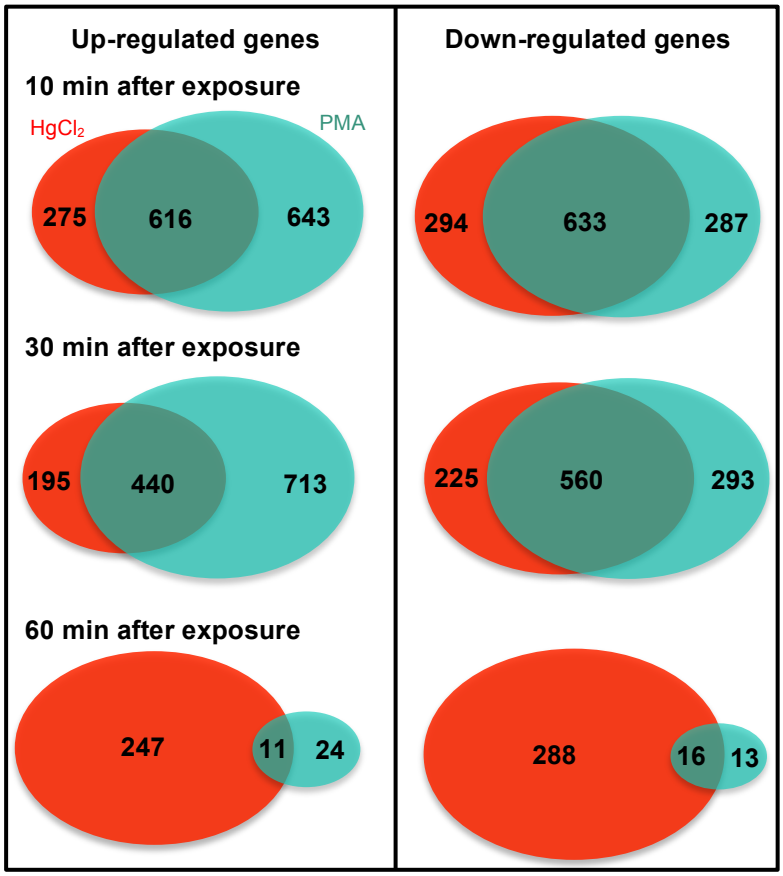

Figure 2: Overlap between differentially expressed genes at each sampling time

The 3 μM $HgCl_2$ exposure is in red and the 3 μM PMA exposure in green. Ovals are to scale only at each time point, but not between between time points in a panel nor between left and right panels.

bioRxiv preprint doi: https://doi.org/10.1101/161646; this version posted July 10, 2017. The copyright holder for this preprint (which was not certified by peer review) is the author/funder, who has granted bioRxiv a license to display the preprint in perpetuity. It is made available under aCC-BY-NC-ND 4.0 International license.

1531

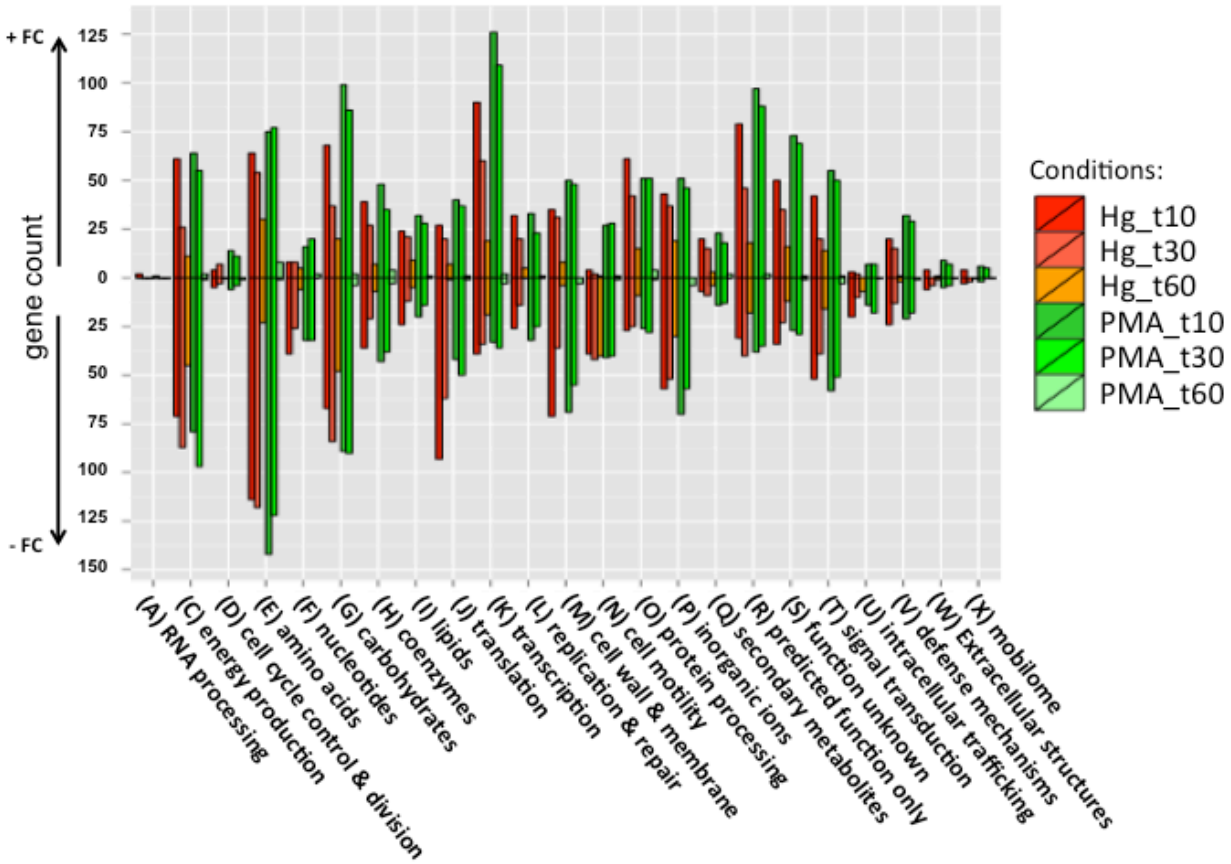

1532

1533 **Figure 3: Counts of differentially expressed genes for each condition grouped by**

1534 **COG functional category.** Genes with a $\log_2$ fold-change ≥ 1 for each condition were

1535 grouped by COG group. Positive counts represent observed up-regulated genes and

1536 negative counts represent observed down-regulated genes. COG code, number of

1537 proteins encoded by genome and category description: (A, 2) RNA processing and

1538 modification; (C, 284) Energy production and conversion; (D, 39) Cell cycle control, cell

1539 division, chromosome partitioning; (E, 355) Amino acid transport and metabolism; (F,

1540 107) Nucleotide transport and metabolism; (G, 381) Carbohydrate transport and

1541 metabolism; (H, 179) Coenzyme transport and metabolism; (I, 121) Lipid transport and

1542 metabolism; (J, 236) Translation, ribosomal structure and biogenesis; (K, 294)

bioRxiv preprint doi: https://doi.org/10.1101/161646; this version posted July 10, 2017. The copyright holder for this preprint (which was not certified by peer review) is the author/funder, who has granted bioRxiv a license to display the preprint in perpetuity. It is made available under aCC-BY-NC-ND 4.0 International license.

Transcription; (L, 139) Replication, recombination and repair; (M, 242) Cell wall, membrane and envelope biogenesis; (N, 102) Cell motility; (O, 156) Post-translational modification, protein turnover, chaperones; (P, 223) Inorganic ion transport and metabolism; (Q, 68) Secondary metabolites biosynthesis, transport and catabolism; (R, 261) General function prediction only; (S, 203) Function unknown; (T, 191) Signal transduction mechanisms; (U, 50) Intracellular trafficking, secretion, and vesicular transport; (V, 91) Defense mechanisms; (W, 31) Extracellular structures; (X, 60) Mobilome, prophages, transposons.

bioRxiv preprint doi: https://doi.org/10.1101/161646; this version posted July 10, 2017. The copyright holder for this preprint (which was not certified by peer review) is the author/funder, who has granted bioRxiv a license to display the preprint in perpetuity. It is made available under aCC-BY-NC-ND 4.0 International license.

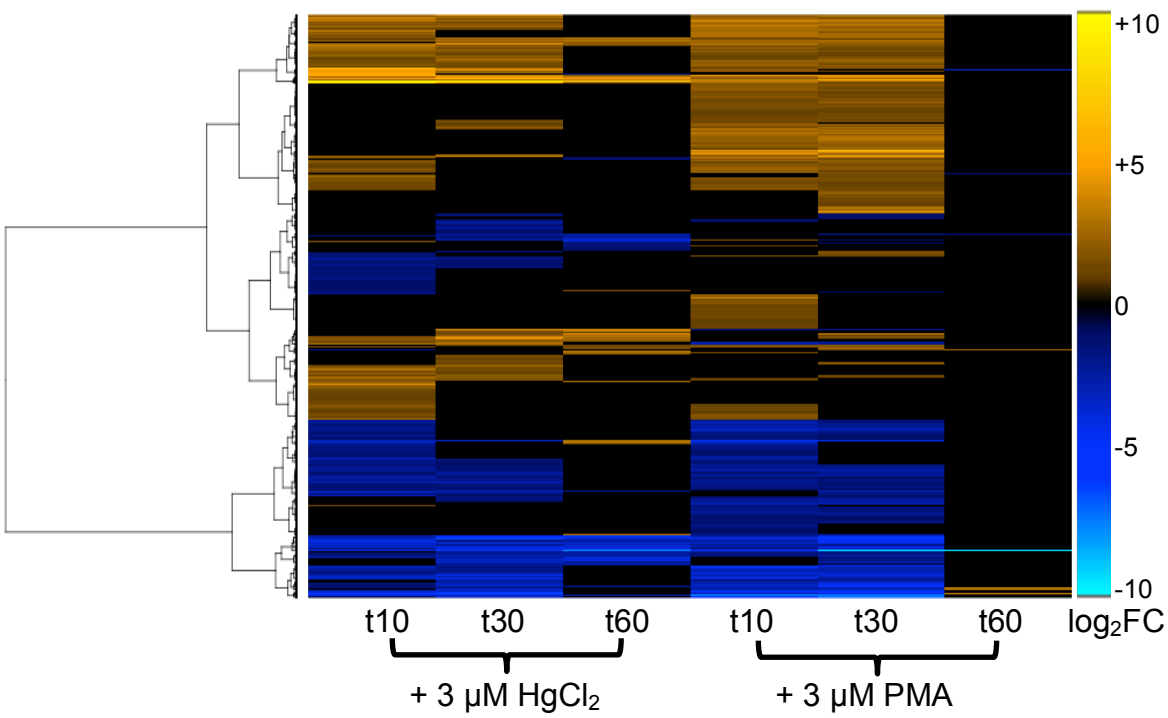

Figure 4: Differentially expressed genes at each RNA sampling time. Heat map of all genes that were differentially expressed in at least one mercury exposure condition (n = 3,149). Genes were clustered by row using Ward's minimum variance method [36] with non-squared $\log_2$ fold-change input values.

bioRxiv preprint doi: https://doi.org/10.1101/161646; this version posted July 10, 2017. The copyright holder for this preprint (which was not certified by peer review) is the author/funder, who has granted bioRxiv a license to display the preprint in perpetuity. It is made available under aCC-BY-NC-ND 4.0 International license.

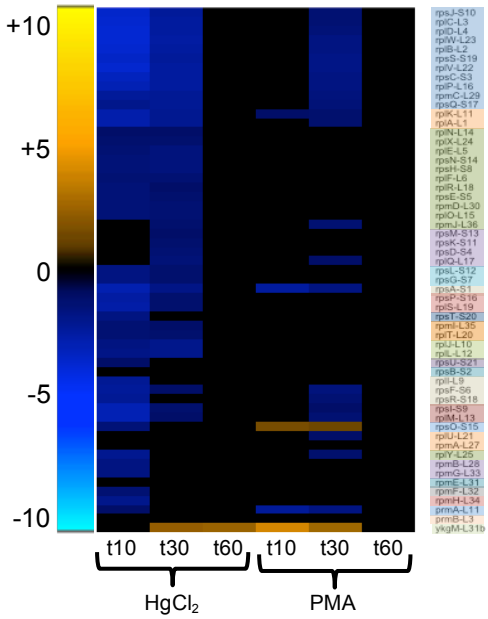

Figure 5: Ribosomal subunit protein genes. Genes are grouped and colored by operon (see larger Figure S11 and Table S13 for details).

bioRxiv preprint doi: https://doi.org/10.1101/161646; this version posted July 10, 2017. The copyright holder for this preprint (which was not certified by peer review) is the author/funder, who has granted bioRxiv a license to display the preprint in perpetuity. It is made available under aCC-BY-NC-ND 4.0 International license.

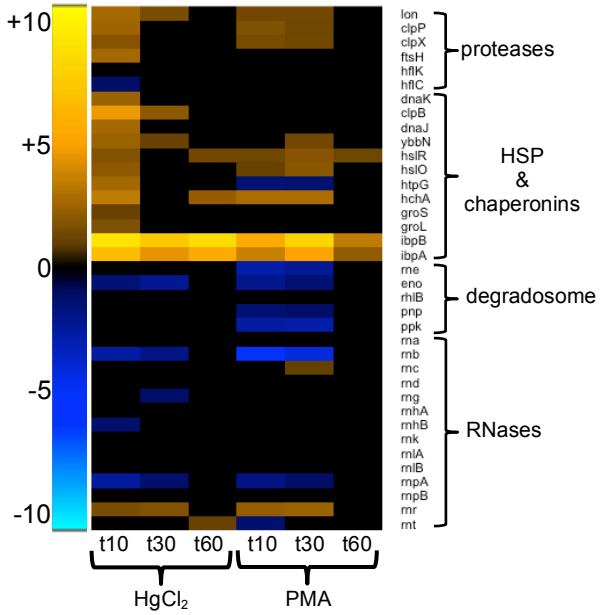

Figure 6: Protein and RNA turnover and repair. (see larger Figure S12 and Table S13 for details).

bioRxiv preprint doi: https://doi.org/10.1101/161646; this version posted July 10, 2017. The copyright holder for this preprint (which was not certified by peer review) is the author/funder, who has granted bioRxiv a license to display the preprint in perpetuity. It is made available under aCC-BY-NC-ND 4.0 International license.

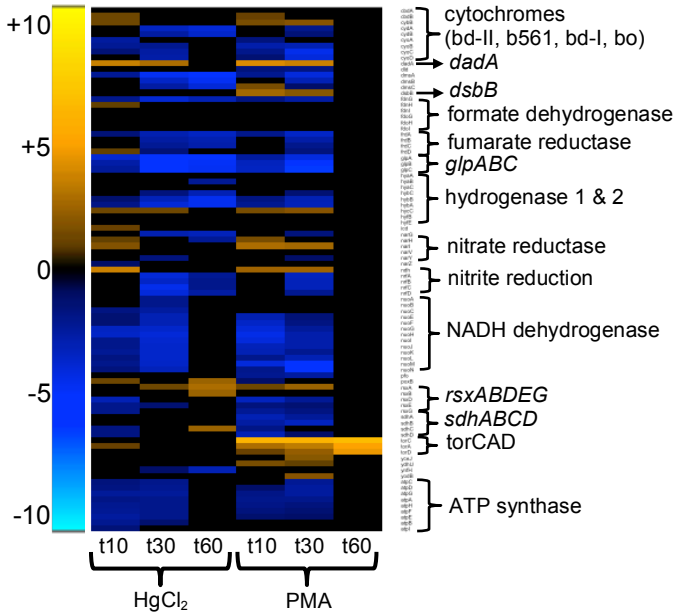

Figure 7: Electron transport chain and ATP-synthase. (see larger Figure S13 and Table S13 for details).

bioRxiv preprint doi: https://doi.org/10.1101/161646; this version posted July 10, 2017. The copyright holder for this preprint (which was not certified by peer review) is the author/funder, who has granted bioRxiv a license to display the preprint in perpetuity. It is made available under aCC-BY-NC-ND 4.0 International license.

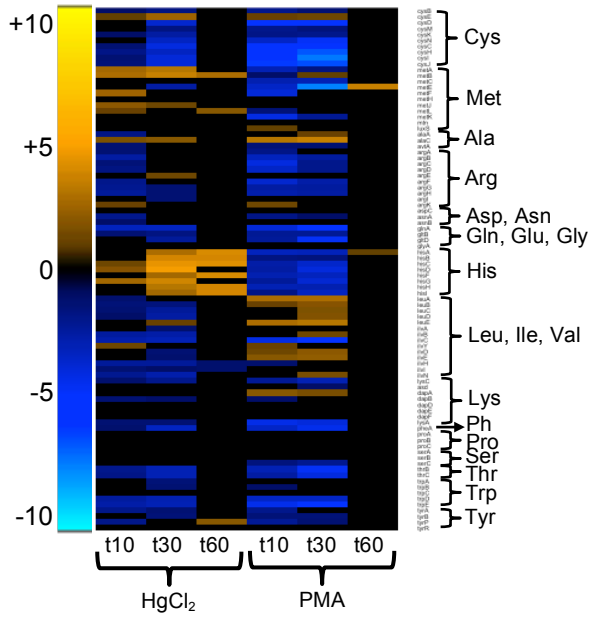

Figure 8: Amino acid biosynthesis. (see larger Figure S22 and Table S13 for details).

bioRxiv preprint doi: https://doi.org/10.1101/161646; this version posted July 10, 2017. The copyright holder for this preprint (which was not certified by peer review) is the author/funder, who has granted bioRxiv a license to display the preprint in perpetuity. It is made available under aCC-BY-NC-ND 4.0 International license.

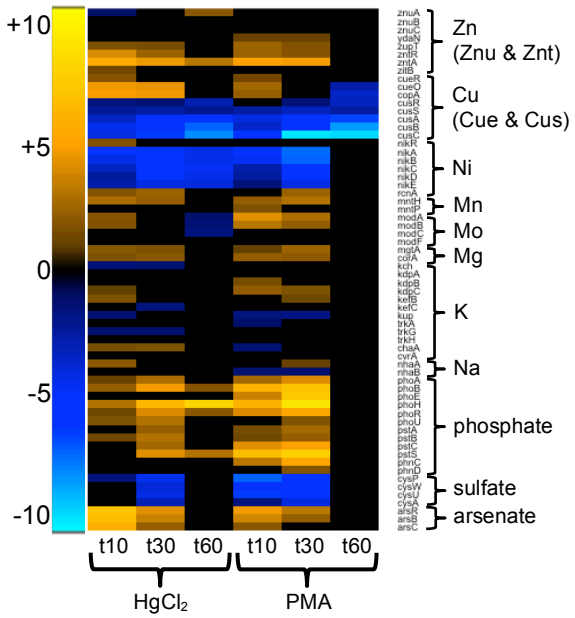

Figure 9: Non-ferrous metals homeostasis. (see larger Figure S23 and Table S13 for details).

bioRxiv preprint doi: https://doi.org/10.1101/161646; this version posted July 10, 2017. The copyright holder for this preprint (which was not certified by peer review) is the author/funder, who has granted bioRxiv a license to display the preprint in perpetuity. It is made available under aCC-BY-NC-ND 4.0 International license.

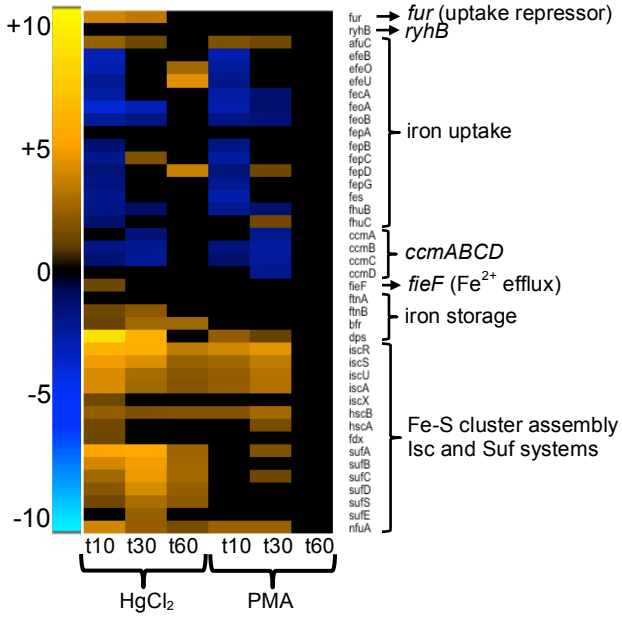

Figure 10: Iron homeostasis. (see larger Figure S24 and Table S13 for details).

bioRxiv preprint doi: https://doi.org/10.1101/161646; this version posted July 10, 2017. The copyright holder for this preprint (which was not certified by peer review) is the author/funder, who has granted bioRxiv a license to display the preprint in perpetuity. It is made available under aCC-BY-NC-ND 4.0 International license.

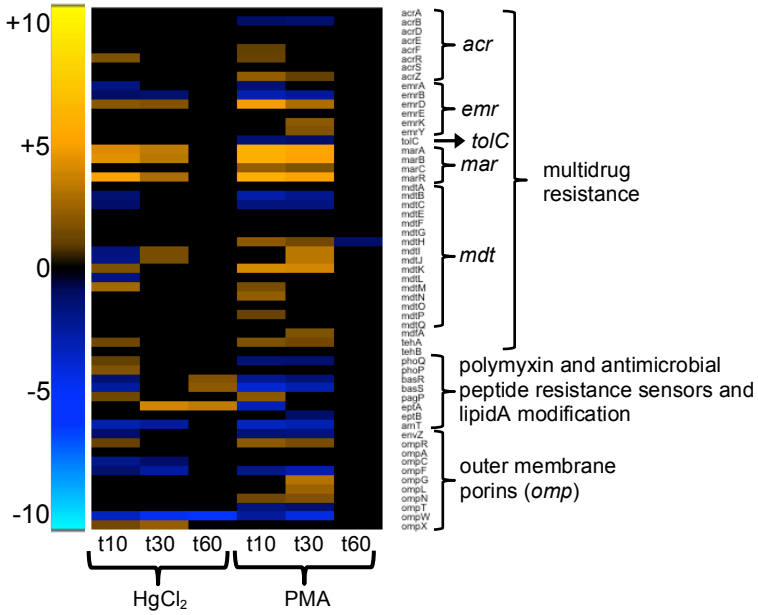

Figure 11: Antibiotic resistance and outer membrane porins. (see larger Figure S26 and Table S13 for details).

bioRxiv preprint doi: https://doi.org/10.1101/161646; this version posted July 10, 2017. The copyright holder for this preprint (which was not certified by peer review) is the author/funder, who has granted bioRxiv a license to display the preprint in perpetuity. It is made available under aCC-BY-NC-ND 4.0 International license.

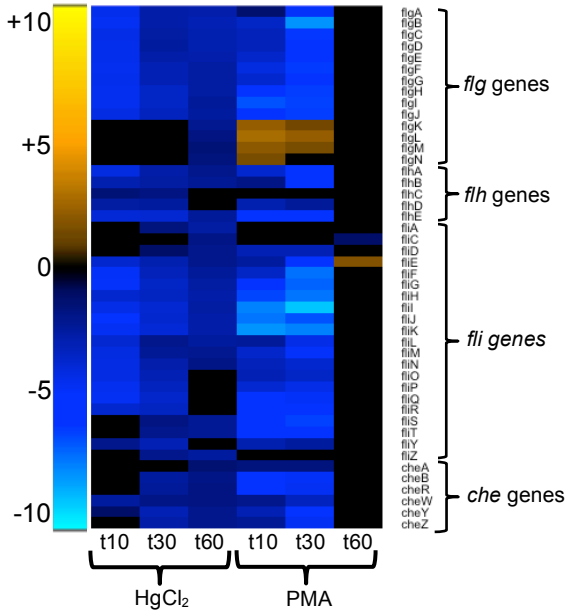

Figure 12: Flagella components and chemotaxis. (see larger Figure S27 and Table S13 for details).

bioRxiv preprint doi: https://doi.org/10.1101/161646; this version posted July 10, 2017. The copyright holder for this preprint (which was not certified by peer review) is the author/funder, who has granted bioRxiv a license to display the preprint in perpetuity. It is made available under aCC-BY-NC-ND 4.0 International license.

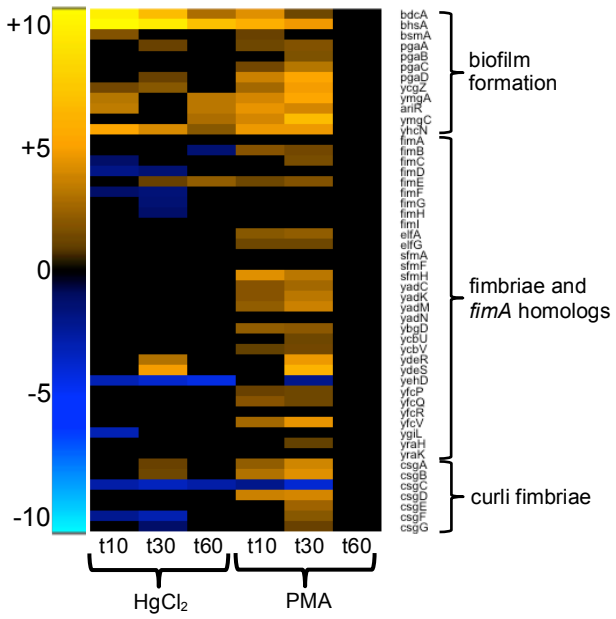

Figure 13: Biofilm formation and fimbriae. (see larger Figure S28 and Table S13 for details).

bioRxiv preprint doi: https://doi.org/10.1101/161646; this version posted July 10, 2017. The copyright holder for this preprint (which was not certified by peer review) is the author/funder, who has granted bioRxiv a license to display the preprint in perpetuity. It is made available under aCC-BY-NC-ND 4.0 International license.

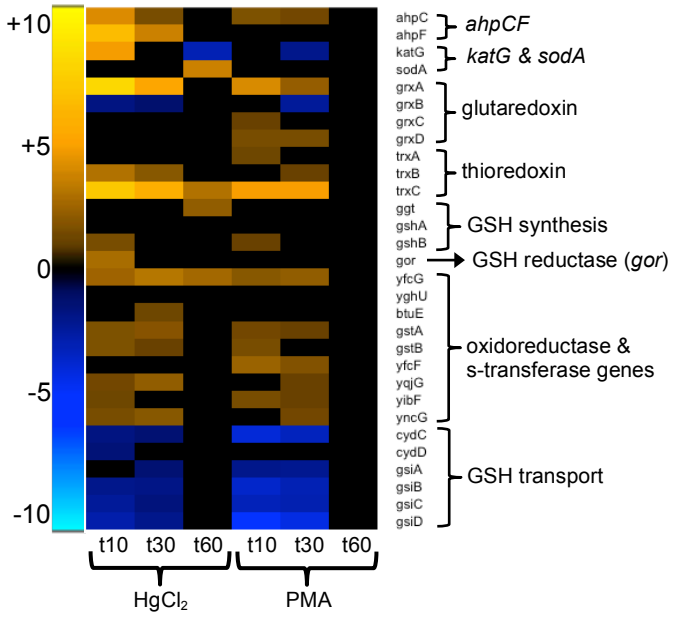

Figure 14: Oxidative stress defense and thiol homeostasis. (see larger Figure S29 and Table S13).